# Overview of SLOPE I and II campaigns: aerosol properties retrieved with lidar and sun-sky photometer measurements

Jose Antonio Benavent-Oltra[1,2,3], Juan Andrés Casquero-Vera[2,3], Roberto Román[4], Hassan Lyamani[2,3], Daniel Pérez-Ramírez[2,3], María José Granados-Muñoz[2,3], Milagros Herrera[5], Alberto Cazorla[2,3], Gloria Titos[2,3], Pablo Ortiz-Amezcua[2,3], Andrés Esteban Bedoya-Velásquez[3,6], Gregori de Arruda Moreira[3,7], Noemí Pérez[8], Andrés Alastuey[8], Oleg Dubovik[5], Juan Luis Guerrero-Rascado[2,3], Francisco José Olmo-Reyes[2,3] and Lucas Alados-Arboledas[2,3]

[1]Department of Civil, Chemical and Environmental Engineering, University of Genoa, Genoa, Italy.
[2]Department of Applied Physics, Universidad de Granada, Granada, Spain.
[3]Andalusian Institute for Earth System Research, IISTA-CEAMA, Granada, Spain.
[4]Group of Atmospheric Optics (GOA-UVa), Universidad de Valladolid, Valladolid, Spain.
[5]Laboratoire d'Optique Atmosphérique (LOA), UMR8518 CNRS, Université de Lille, Villeneuve D'ASCQ, France.
[6]The French Aeorospace Lab, ONERA, Toulouse, France.
[7]Federal Institute of São Paulo (IFSP), São Paulo, Brazil.
[8]Institute of Environmental Assessment and Water Research (IDAEA), CSIC, Barcelona, Spain.

*Correspondence to:* Jose Antonio Benavent-Oltra (jbenavent@ugr.es)

**Abstract.** The Sierra Nevada Lidar aerOsol Profiling Experiment I and II (SLOPE I and II) campaigns were intended to determine the vertical structure of the aerosol by remote sensing instruments and test the various retrieval schemes for obtaining aerosol microphysical and optical properties with in-situ measurements. The SLOPE I and II campaigns were developed along summer 2016 and 2017, respectively, combining active and passive remote sensing with in-situ measurements at the stations belonging to AGORA observatory (Andalusian Global ObseRvatory of the Atmosphere) in the Granada area (Spain). In this work, we use the in-situ measurements of these campaigns to evaluate aerosol properties retrieved by GRASP code (Generalized Retrieval of Atmosphere and Surface Properties) combining lidar and sun-sky photometer measurements. We show an overview of aerosol properties retrieved by GRASP during SLOPE I and II campaigns. Besides, we evaluate the GRASP retrievals of total aerosol volume concentration (discerning between fine and coarse modes), extinction and scattering coefficients, and for the first time we present an evaluation of absorption coefficient.

The statistical analysis of the aerosol optical and microphysical properties, both column-integrated and vertically-resolved, from May to July 2016 and 2017 shows a large variability in aerosol load and types. The results show a strong predominance of desert dust particles due to the North African intrusions. The vertically-resolved analysis denotes a decay of the atmospheric aerosols with altitude up to 5 km a.s.l. Finally, desert dust and biomass burning events were chosen to show the high potential of GRASP to retrieve vertical profiles of aerosol properties (e.g., absorption coefficient and single scattering albedo) for different

aerosol types. The aerosol properties retrieved by GRASP show good agreement with simultaneous in-situ measurements (nephelometer, aethalometer, Scanning Mobility Particle Sizer and Aerodynamic Particle Sizer) performed at Sierra Nevada Station (SNS) in Granada. In general, GRASP overestimates the in-situ data at SNS with a mean difference lower than 6 $\mu m^3/cm^3$ for volume concentration, 11 $Mm^{-1}$ and 2 $Mm^{-1}$ for scattering and absorption coefficient. On the other hand, the comparison of GRASP with airborne measurements also shows an overestimation with mean absolute differences of $14 \pm 10$ $Mm^{-1}$ and $1.2 \pm 1.2$ $Mm^{-1}$ for scattering and absorption coefficients, showing a better agreement for absorption (scattering) coefficient with higher (lower) aerosol optical depth. The potentiality of GRASP showed in this study will contribute to enhancing the representativeness of the aerosol vertical distribution and provide information for satellite and global model evaluation.

## 1.    Introduction

The characterization of atmospheric aerosol optical and microphysical properties is difficult due to their high spatial and temporal variability in the atmosphere. These together with the complexity of the aerosol-radiation interaction (scattering and absorbing incident solar and outgoing thermal radiation) and the cloud-aerosol interaction (modifying cloud properties), results in a large uncertainty in the radiative forcing of climate due to aerosols (IPCC, 2013).

During the last decades, a good number of field campaigns has been carried out for studying atmospheric aerosol properties (e.g., Tanré et al., 2003; Mallet et al., 2016; Veselovskii et al., 2016; Vandenbussche et al., 2020) using observatories with in-situ measurements and included in global networks, based on passive and active remote sensing instruments, such as AERosol RObotic NETwork (AERONET; Holben et al., 1998) and European Aerosol Research LIdar NETwork (EARLINET; Pappalardo et al., 2014). On the one hand, the in-situ ground-based observatories only represent limited atmospheric sample in the layer closest to the surface. The passive remote sensing instruments, such as sun-sky photometers or satellites provide aerosol properties in entire atmospheric column, while they have very limited information about variations within the column. Hence, vertically-resolved aerosol observations are needed to discern between the different aerosol layers and to study their radiative properties. In these regards, the lidar systems are used for aerosol optical and microphysical properties profiling. Basic lidar systems only have information on the backscatter elastic signals which allow the retrieval of aerosol backscatter coefficient ($\beta$) vertical profiles by the Klett–Fernald method (Fernald et al., 1972; Fernald, 1984; Klett, 1981, 1985) assuming a constant aerosol lidar ratio (LR). However, advanced lidar systems provide

information on the backscatter elastic and inelastic signals allowing the retrieval of vertical profiles of aerosol backscatter and extinction ($\alpha$) coefficients by the Raman technique (e.g., Ansmann et al., 1992; Whiteman et al., 1992). These measurements allow retrieving the particle vertical microphysical properties by inversion algorithms using the $3\beta + 2\alpha$ configuration (e.g., Müller et al., 1999; Böckmann, 2001; Veselovskii et al., 2002).

The main drawback of these algorithms is the scarcity of Raman lidar measurements during the daytime that represents a limitation to the retrievals of the extinction coefficient data (Veselovkii et al., 2015; Ortiz Amezcua et al., 2020). As an alternative, during the last years, several synergetic retrievals algorithms have been developed to retrieve aerosol optical and microphysical properties combining data from sun-sky photometers and backscatter lidar measurements such as LIRIC (LIdar-Radiometer Inversion Code) by Chaikovsky et al. (2008, 2016, Granados-Muñoz et al, 2020) and GARRLiC (Generalized Aerosol Retrieval from Radiometer and Lidar Combined data) by Lopatin et al. (2013). One of the most popular advanced inversion algorithms is the Generalized Retrieval of Atmosphere and Surface Properties code (GRASP; Dubovik et al., 2011, 2014). It should be noted here that GARRLiC is a branch of GRASP. The versatility of GRASP allows the retrieval of aerosol vertical and surface properties combining different types of measurements, such as sun-photometers, lidar, ceilometers, satellite, sky-cameras, nephelometers, etc. (e. g. Lopatin et al., 2013; Espinosa et al., 2017; Román et al., 2017; Torres et al., 2017; Benavent-Oltra et al., 2017; Titos et al., 2019 Herreras et al., 2019; Dubovik et al., 2019). The aerosol properties retrieved by GRASP have been evaluated in previous works using as reference the volume concentration provided by LIRIC algorithm (differences ~20%; Benavent-Oltra et al., 2017), the backscatter and extinction coefficients calculated with Klett-Fernald and Raman methods (differences below 30%; Benavent-Oltra et al., 2017, 2019; Tsekeri et al., 2017). In addition, GRASP retrievals have been used to evaluate forecast models, as constrains for global models and as inputs for radiative transfer models (e.g., Tsekeri et al., 2017; Chen et al., 2018, 2019; Granados-Muñoz et al., 2019). It is important to explore the potential of this kind of algorithms by applying them to different input data and for different atmospheric conditions. In these regards, the extensive measurement dataset obtained during Sierra Nevada Lidar aerOsol Profiling Experiment I and II (SLOPE I and SLOPE II) campaigns in May, June and July 2016 and 2017, respectively, allows an evaluation of the atmospheric aerosol properties retrieved by GRASP code combining lidar and sun-sky photometer measurements. This database was successfully

utilized in several previous studies of the atmospheric aerosol (e.g., de Arruda Moreira et al., 2018, 2019; Bedoya-Velásquez et al., 2018; Horvath et al., 2018; Casquero-Vera et al., 2020).

The main objective of this work is to provide an overview of the aerosol optical and microphysical properties during SLOPE I and II campaigns using the GRASP code. We check the GRASP retrievals versus in-situ measurements performed at the Sierra Nevada Station (SNS, Spain; 2500 m a.s.l.) and instrumented flights. This is the first long-term evaluation of GRASP that combines sun-sky photometer and multi-wavelength lidar measurements to retrieve profiles of aerosol intensive properties separately for both fine and coarse modes instead of only one mode such as using ceilometer measurements (e.g., Román et al., 2018; Titos et al., 2019). In addition, a statistical analysis of both total column and vertically-resolved aerosol properties is performed, and two extreme events of desert dust and biomass burning are evaluated.

## 2.    Sites and measurements

The SLOPE I and II campaigns took place in Granada (Spain) during the summers of 2016 and 2017 and were designed to determine the vertical structure of the aerosol by remote sensing instruments through the application of various retrieval schemes for obtaining aerosol microphysical and optical properties. The main objective of this campaign was to perform a closure study by comparing remote sensing system retrievals of atmospheric aerosol properties with various in-situ measurements (Román et al., 2017; Benavent-Oltra et al., 2019). The study area typically presents variable aerosol loads and type, with large presence of anthropogenic aerosols mainly in winter (e.g., Lyamani et al., 2010; del Aguila et al., 2018; Casquero-Vera et al., 2021) and frequent Saharan dust intrusions (e.g., Perez-Ramirez et al., 2012; Valenzuela et al., 2012) and primary aerosol associated to the local phenology (Cariñanos et al., 2020). The region is often affected by episodes of aerosol stagnation due to its complex geography (e.g., Lyamani et al., 2010), while Atlantic air masses are usually responsible for cleaning the atmosphere (Perez-Ramirez et al., 2016).

During SLOPE I and II the instrumentation was deployed at the three stations of the AGORA (Andalusian Global ObseRvatory of the Atmosphere) observatory. The main station of AGORA is in the Andalusian Institute for Earth System Research / IISTA-CEAMA (UGR; 37.16º N, 3.61º W; 680 m a.s.l.) in the city of Granada. UGR station operates many remote sensing and in-situ instrumentation, mostly in the framework of ACTRIS (Aerosols, Clouds, and Trace gases Research InfraStructure Network, https://www.actris.eu/default.aspx) research

infrastructure. The other two stations of AGORA observatory are in the Sierra Nevada Mountain range: Cerro Poyos (CP; 37.11º N, 3.49º W; 1820 m a.s.l.) and Sierra Nevada Station (SNS; 37.10º N, 3.39º W, 2500 m a.s.l.). SNS is located ~20 km southeast of Granada city and 1.8 km above UGR station (see Figure 1 in Herreras et al., 2019 for details). During SLOPE field campaigns, a large set of in-situ instrumentation was deployed at SNS station and on-board the Partenavia P68 airplane. The in-situ measurements allowed the validation of aerosol optical and microphysical properties obtained by remote sensing techniques at the UGR station. Table 1 summarizes the main instrumentation operating in UGR, SNS and on-board the airplane.

**[Table 1]**

### 2.1.    Remote sensing instrumentation

The UGR station is equipped with a multi-wavelength Raman lidar system (LR331D400, Raymetrics S.A.), which is included in EARLINET since 2005 and contributes to the ACTRIS research infrastructure. This instrument is composed of a Nd:YAG pulsed laser that emits at 1064 nm (110 mJ per pulse), 532 nm (65 mJ per pulse) and 355 nm (60 mJ per pulse). The detection branch has seven channels: four to measure the backscattered light at 355, 532 (parallel and perpendicular components) and 1064 nm; two channels at 353.9 and 530.2 nm (387 and 607 nm until December 2016; Ortiz-Amezcua et al., 2020) for the detection of Raman scattering from $N_2$, and one channel to detect the water vapour Raman scattering at 408 nm. More information of this instrument can be found in Guerrero-Rascado et al. (2008, 2009) and Ortiz-Amezcua et al. (2020).

Each station of AGORA is equipped with a sun-sky photometer CE-318 (Cimel Electronique S.A.S.) that operates in frame of the AERONET network. This instrument performs measurements of sun direct irradiance, which is used to derive the aerosol optical depth (AOD) usually at 340, 380, 440, 500, 675, 870 and 1020 nm, and sky radiance in almucantar configuration at 440, 675, 870 and 1020 nm. The instruments at UGR and SNS during SLOPE I and II were sun-sky-lunar photometer Cimel CE318-T, which also perform lunar direct irradiance measurements to retrieve the AOD during night-time between the first and third Moon quarters (e.g., Barreto et al. 2016, 2019, Román et al., 2020). In this work, we used AERONET Version 3 Level 1.5 (cloud-screened) data (e.g., Giles et al., 2019; Sinyuk et al., 2020).

The ground-based MWR (RPG-HATPRO G2, Radiometer physics GmbH) located at UGR station as part of the MWRnet (Rose et al., 2005; Caumont et al., 2016), is used here for retrieving temperature profiles. MWR is a passive remote sensor that performs unattended measurements of the temperature brightness of oxygen and water vapor in the atmosphere. The oxygen is measured in the K-band (51-58 GHz) and the water vapor in the V-band from 22 to 31 GHz with a radiometric resolution between 0.3 and 0.4 rms errors at 1.0 s integration time. The retrievals of temperature profiles from the measured brightness temperatures are performed using a standard feed forward neural network (Rose et al., 2005). The uncertainty of the MWR temperature profiles varies according to the weather conditions (cloud-free or cloudy), ranging between 1.8 K and 3 K (Bedoya et al., 2019). A detailed description of this system can be found in Navas-Guzmán et al. (2014) and Bedoya et al. (2018, 2019).

### 2.2. In-situ instrumentation

The integrating nephelometer (model TSI 3563) at SNS measures the particle light scattering coefficient ($\sigma_{sca}$) at three wavelengths (450, 550 and 700 nm) with 1-min temporal resolution. The aerosol flow in the nephelometer was set to 30 lpm. The nephelometer measurements are within the angular range 7-170º, so the data were corrected for truncation and non-Lambertian illumination errors (Anderson and Ogren, 1998). The Aethalometer AE-33 (Magee Scientific Company, 206 Berkeley, USA) is based on filter technique and provides aerosol absorption coefficient ($\sigma_{abs}$) at seven wavelengths (370, 470, 520, 590, 660, 880 and 950 nm). The aethalometer was intercompared with other similar systems during the ACTRIS inter-comparison (ACTRIS 2 Absorption Photometer Workshop, September 2015, Leipzig, Germany), which assures the data quality. The combination of integrating nephelometer and aethalometer data allows the calculation of the aerosol extinction coefficients ($\alpha$).

The Scanning Mobility Particle Sizer (SMPS) composed of an Electrostatic Classifier (TSI Mod. 3082) and a Condensation Particle Counter (CPC; TSI Mod. 3772), provides the sub-micron particle number size distribution within the 6–307.5 nm particle mobility radius range with 5-min temporal resolution. SMPS data have been corrected of internal diffusion losses and multiple charges by AIM software (version 10.2.0, TSI, Inc., St Paul MN, USA). The SMPS measurements followed ACTRIS and GAW recommendations (Wiedensohler et al., 2012, 2018) and high-quality data were guaranteed after the successful participation of the instrument in the ACTRIS inter-comparisons workshops (TROPOS, Leipzig, Germany) and in-situ intercomparison (ACTRIS Round Robin Tour). The Aerodynamic Particle Sizer (APS; TSI Mod. 3321) provides the coarse particle number size distribution within the 0.25–10 µm

aerodynamic radius range. The APS also measures number aerosol concentrations up to 1000 particles·cm$^{-3}$ with coincidence errors inferior to 5% and 10% at 0.25 and 5 μm radius, respectively. By the combination of SMPS and APS measurements, total aerosol volume concentrations were obtained in the 0.05–10 μm radius range with 5-min time resolution. Since SMPS and APS measurement principles are based on mobility and aerodynamic particles properties, conversion from aerodynamic to mobility diameter is needed to combine both measurements. In this sense, both measurements could be related by a factor Q (Sorribas et al., 2015) that depends on chemistry and aerosol shape. Due to the absence of information of both properties, Q-value=1 has been assumed for conversion from aerodynamic to mobility size distribution (mobility diameter equal to aerodynamic diameter).

### 2.3.    Aircraft instrumentation

During the campaigns, dedicated flights with an airplane (Partenavia P68) equipped with in-situ instrumentation were carried out over the study area between 15th and 18th June 2016 for SLOPE I, and between 21st and 24th June 2017 for SLOPE II campaigns. The aircraft campaigns consisted of 3 flights each year. Figure 1 shows the spiral trajectories of one flight, each flight consisted of several ascending and descending spiral profiles centred on the location of the UGR station. The radius of the spirals were about 500 meters. On each flight, only ascending profiles were used in the following analysis. To avoid the potential partial sampling of the exhaust of the aircraft, the descending profiles were performed on a different location.

**[Figure 1]**

Air flows to the instruments through a near-isokinetic isoaxial inlet designed by Aerosol d.o.o. (www.aerosol.si) at a flow rate of 10 lpm. The main flow is divided by two flow splitters that divide the sampled air among the instruments. Yus-Díez et al. (2020) reported minimal losses in the inlet system for small particles, while larger differences were observed for particles with radius >2-2.5 μm. The Ecotech Aurora nephelometer is an integrating nephelometer that measures the particle light scattering coefficient at three wavelengths (450, 525 and 635 nm) with a time resolution of 10 seconds. This instrument measures the scattering coefficient in the angular range 10-170º, and the correction of Müller et al. (2011) was used to account for the angular truncation errors. The Aethalometer AVIO AE33 (Aerosol d.o.o.) is the aircraft version of the Aethalometer AE-33 described above. Using the same measurement principle (Drinovec et al., 2015) it provides particle absorption coefficients at seven wavelengths (370, 470, 520, 590, 660, 880 and 950 nm) with a time resolution of 1 second.

The position of the aircraft was tracked using a GPS and all instruments on-board the aircraft were time-synchronized. Further information on the aircraft instrumentation can be found in Yus-Díez et al. (2020).

## 3. Methodology

### 3.1. GRASP retrievals

In this work, we use the GRASP code following the scheme proposed by Lopatin et al. (2013), which combines lidar and sun-sky photometer measurements to retrieve the optical and microphysical properties of aerosol particles. This scheme uses normalized backscattered range corrected signal at 355, 532 and 1064 nm from lidar, the AOD and sky radiance (almucantar scan) both at 440, 675, 870 and 1020 nm from AERONET version 3 level 1.5. It should be noted that GRASP retrievals were performed during daytime with solar zenith angles larger than 40º and clear-sky conditions. This configuration of GRASP allows the retrieval of aerosol properties for both fine (radii range 0.05 to 0.576 µm) and coarse (radii range 0.33 to 15 µm) modes separately, the complex refractive index, single-scattering albedo (SSA) and lidar ratio (LR). Besides, GRASP provides vertical concentration of fine and coarse mode separately, and the vertically-resolved profiles of the extinction, absorption and scattering coefficients, SSA, LR, Ångström exponent of absorption (AAE) and scattering (SAE).

Individual GRASP retrievals are performed for each sky radiance almucantar sequence available from AERONET with correlative lidar measurements in a ±15 min time window. Specifically, the normalized lidar range corrected signal profile used in each retrieval is previously 30-min averaged and computed for 60 log-spaced heights between minimum and maximum heights as proposed by Lopatin et al. (2013). Here, the minimum height has been chosen as 400 m above the ground to minimize the effect of incomplete overlap and maximum height as 6000 m above the ground to have higher signal-to-noise ratio. This GRASP configuration is described in detail in Benavent-Oltra et al. (2019). The data used in this study were recorded between May and July of 2016 and 2017 with 286 retrievals in 69 days that passed the filter imposed to the inversion process (relative residual < 15 %; Torres et al., 2017).

### 3.2. Aircraft data

In order to make comparable the profiles from the aircraft data and the remote sensing retrievals, there are some corrections to consider. Remote sensing data are provided at ambient conditions (temperature and pressure), but the aircraft data is registered at different conditions. Nephelometer data from the aircraft were recorded at cabin temperature and ambient pressure,

and aethalometer data were registered at 0ºC and 1013.25 hPa. The cabin temperature used was the nephelometer sampling temperature ($T_s$), i.e. temperature inside the nephelometer, and the profile atmospheric pressure used was the nephelometer pressure sensor ($P_s$). The cabin on the aircraft was not pressurized so the pressure inside the nephelometer can be consider the outside pressure. The aircraft did not register the outside temperature, so an external source of temperature profile was required. We used a temperature profile from a microwave radiometer MWR ($T_{mwr}$) as described in section 2.1., using an average profile during the time of the entire aircraft profile and interpolated to the exact altitudes of the aircraft profile.

Aircraft profiles show some noise, especially at higher altitudes, so a convolution with a mean filter was applied to the aircraft in-situ data in order to smooth the profiles. We observed that using 100 meters for the nephelometer and 200 meters for the aethalometer data in the vertical profiles reduced noise while preserving the profile features. Finally, Aurora nephelometer wavelengths were converted to the TSI wavelengths using the Ångström exponent law to make the aircraft and ground based in-situ data comparable.

## 4.    Results

### 4.1.    Evaluation of GRASP retrievals versus in-situ data

#### 4.1.1.  At high mountain station

For the inter-comparison between GRASP retrievals and SNS in-situ data, we selected the in-situ measurements averaged in ±15 min around the GRASP retrieval time and the 400 m averaged data of GRASP retrieval profile at 2500 m a.s.l. (SNS altitude). The number of coincident GRASP retrievals with in-situ measurements are 231, 202, 154 and 151 for volume concentration, $\sigma_{sca}$, $\sigma_{abs}$ and $\alpha$ coefficients, respectively. Therefore, the results and discussion about the comparison between GRASP and SNS in-situ measurements are referred exclusively to this height range.

Figure 2 shows the aerosol total ($VC_T$), fine mode ($VC_F$) and coarse mode ($VC_C$) volume concentration retrieved by GRASP versus those measured with in-situ instruments at SNS. The aerosol volume concentrations at SNS were calculated for the 0.05–0.5 and 0.5–10 μm radius size ranges for the fine and coarse modes, respectively. Due to the sensibility of linear regression to outliers, $VC_T$ concentrations larger than 190 μm$^3$/cm$^3$ (99th percentile) and their corresponding fine and coarse data have been excluded in this analysis. In general, volume concentrations retrieved by GRASP code shows good correlation with SNS measurements with correlation coefficients ($R$) of 0.58, 0.83 and 0.80 for fine, coarse and total volume

concentrations, respectively. The results show that GRASP retrievals overestimate in-situ measurements with a mean difference (±standard deviation) of $4 \pm 4$ μm³/cm³ and $6 \pm 8$ μm³/cm³ for fine and total volume concentrations, respectively. In contrast, better correlation is observed for coarse mode volume concentrations (slope equals to 1) with a lower mean difference ($2 \pm 6$ μm³/cm³). In terms of absolute concentrations, 65% (91%), 70% (88%) and 45% (71%) of the differences are observed within ±5 μm³/cm³ (±10 μm³/cm³) for fine, coarse and total volume concentrations, respectively. These results are similar to those found in previous GRASP assessments by Benavent-Oltra et al. (2017) and Tsekeri et al. (2017). Those authors also showed an overestimation of $VC_F$ compared with in-situ data, while for $VC_C$ similar GRASP retrievals to in-situ data was found for cases with coarse particles predominate. The observed overestimation is lower than the obtained by Román et al. (2018) using GRASP with ceilometer data, and by Benavent-Oltra et al. (2019) using GRASP with lidar emission signals at 355, 532 and 1064 nm. Titos et al. (2019) found that the agreement between GRASP retrievals (from ceilometer measurements) and in-situ data improved when the contribution of fine particles was negligible.

**[Figure 2]**

Figure 3 shows $\sigma_{sca}$ and $\sigma_{abs}$ obtained by GRASP at ~2.5 km height versus those obtained by in-situ measurements at SNS. The comparison has been performed interpolating the GRASP values at 355, 532 and 1064 nm to the wavelengths of the nephelometer (450, 550 and 700 nm) and the aethalometer (370, 520 and 880 nm) by the Ångström exponent law. For the $\sigma_{sca}$, we can observe that generally the agreements between GRASP and in-situ data are similar at the three wavelengths ($R$ ~0.95). The slopes of the linear fits are equal to 1 with an intercept lower than 10 Mm⁻¹ that decreases for larger wavelengths. Globally, GRASP overestimates in-situ data at SNS with a mean difference (±standard deviation) of $11 \pm 17$ Mm⁻¹, $6 \pm 14$ Mm⁻¹ and $4 \pm 11$ Mm⁻¹ at 450, 550 and 700 nm, respectively. On the other hand, for $\sigma_{abs}$, GRASP shows good correlation with the in-situ data with correlation coefficients around 0.85. In general, GRASP overestimates the in-situ data at SNS as shown the slopes (~1.2) and intercepts (from 0.5 to 1.5 Mm⁻¹) of the regressions. The mean differences (±standard deviation) of $\sigma_{abs}$ are $2 \pm 6$ Mm⁻¹, $1 \pm 3$ Mm⁻¹ and $0.8 \pm 1.7$ Mm⁻¹ at 370, 520 and 880 nm, respectively. Furthermore, the differences between GRASP and in-situ measurements are less than ±2.5 Mm⁻¹ for 61%, 81% and 90% of the data at 370, 520 and 880 nm, respectively. The results from Figure 3 for the validation of $\sigma_{sca}$ are similar to previous validations of GRASP retrievals with in-situ data from high mountain sites (e.g., Titos et al., 2019; Benavent-Oltra et

al., 2019). However, it should be noted that the results presented here are the first direct validation of retrieved $\sigma_{abs}$.

330    Finally, the comparison between GRASP retrievals and in-situ data for extinction coefficient at 532 nm showed in Figure 4a evidence better agreement. The in-situ extinction coefficient at 532 nm is the sum of the scattering and absorption coefficients interpolated to 532 nm using the Ångström exponent law. The GRASP retrievals and in-situ data show good agreement (slope equals to 1) and are highly correlated ($R$ = 0.9). Figure 4b shows the

335    frequency histogram of the differences in extinction coefficient ($\Delta\alpha$) between GRASP and in-situ, showing a skewed histogram to positive differences that implies slightly overestimation by GRASP. These overestimations can be associated with the differences in scattering coefficient.

**[Figure 3]**

340    **[Figure 4]**

### 4.1.2. Aircraft profiles

A total of 6 flights were carried out on 15th, 17th and 18th June 2016 during SLOPE I and 21st, 23rd and 24th June 2017 during SLOPE II. During the SLOPE I flights, the aerosol conditions were characterized by AOD values at 440 nm (AOD$_{440}$) lower than 0.1 and Ångström exponent

345    (AE), computed with AOD at 440 and 870 nm (AE$_{440-870}$), between 0.6 and 1.3. On the other hand, during the week of flights in the SLOPE II there was a dust intrusion from Sahara Desert with higher AOD$_{440}$ values (ranging from 0.13 to 0.36 on 23rd and 24th June 2017, respectively) and low AE$_{440-870}$ values between 0.3 and 0.8. Figure 5 shows the vertical profiles of scattering and absorption coefficients retrieved by GRASP code and measured by the on-board

350    instrumentation. This figure also includes the mean value measured at SNS station during the flights. For the sake of comparison, the GRASP values at 355, 532 and 1064 nm has been interpolated to the nephelometer and aethalometer wavelengths using the Ångström exponent law.

**[Figure 5]**

355    For $\sigma_{sca}$, both GRASP and airborne measurements follow the same pattern where GRASP overestimates the airborne data with a mean absolute difference of $14 \pm 10$ Mm[-1]. During SLOPE I, these mean absolute differences are lower than 8 Mm[-1] and there is a good agreement between GRASP and SNS measurements (differences <4 Mm[-1]). However, during

SLOPE II, the differences between GRASP and in-situ measurements (both airborne and SNS) are larger, reaching values of 30 Mm$^{-1}$. In the case of $\sigma_{abs}$, GRASP and airborne profiles show large differences during SLOPE I with mean absolute differences between 0.5 and 3 Mm$^{-1}$ reaching differences around 6 Mm$^{-1}$ on 18$^{th}$ June 2016. On the other hand, the absorption coefficients retrieved by GRASP show good agreement with in-situ measurements (both airborne and SNS) with a mean absolute difference of 0.7 ± 0.4 Mm$^{-1}$ during SLOPE II. In general, the differences between GRASP and in-situ measurements are close to the detection limit for the aethalometer on-board the airplane and SNS. The differences obtained both for $\sigma_{sca}$ and $\sigma_{abs}$ can be explained due to the low AOD$_{440}$ (below 0.40) that represents a challenge for the retrieval of the aerosol properties both for AERONET (Dubovik and King, 2000; Dubovik et al., 2000) and inversion algorithms as GRASP (Lopatin et al., 2013). However, the very good agreement in absorption coefficient during SLOPE II indicates the good capability of GRASP to retrieve vertical profiles of absorption to AOD$_{440}$ higher 0.1.

### 4.2. Aerosol properties during SLOPE I and II

### 4.2.1. Column-integrated

Figure 6 shows the temporal evolutions of AOD$_{440}$ and AE$_{440-870}$ daily mean values retrieved by GRASP code at UGR during SLOPE I and II campaigns. Daily averaged values of AOD$_{440}$ retrieved by GRASP code ranges from 0.06 to 1.0, with a mean (± standard deviation) value of 0.22 ± 0.18, while AE$_{440-870}$ varies from 0.11 to 1.6 with a mean value of 0.8 ± 0.4. The large variability of AODs and Ångström exponents observed in Figure 6 are typical for this season in the study area (e.g., Perez-Ramirez et al., 2012). Large AODs and low AE values as those observed on 20$^{th}$ July 2016 are related to Saharan dust outbreaks (e.g., Román et al., 2018; Benavent-Oltra et al., 2019), while large AODs and AE values as those observed on 26$^{th}$ July 2017 are related to a biomass burning transport (from Portugal in this case) (Turco et al., 2019).

[Figure 6]

Figure 7 shows the Box-Whisker diagrams of retrieved aerosol columnar-integrated properties such as SSA, LR and aerosol absorption optical depth (AAOD) at 355, 440, 532, 675, 870, 1020 and 1064 nm retrieved by GRASP code during the study period. For aerosol intensive properties, the SSA values are typical for Saharan dust outbreaks at the study region (e.g., Valenzuela et al., 2012), ranging from 0.88 ± 0.05 at 355 nm to 0.90 ± 0.06 at 1064 nm, respectively. These relatively large values of SSA for all wavelengths indicate a small concentration of absorbing aerosol particles (e.g., mineral dust). The LR values show large

wavelength-variability, with mean values ranged from 80 ± 30 sr at 355 nm to 35 ± 16 sr at 1064 nm, being typical for Saharan desert dust (Shin et al., 2018). For aerosol extensive properties, the highest AAODs (>0.10) correspond both to dust and biomass-burning events, with an absorption Ångström exponent (AAE; computed in the spectral range 355-1064 nm) higher than 1.5 for desert dust event and around 1.0 for biomass burning event. The variability in AAE can be explained by the differences in particles chemical compositions (e.g., Russell et al., 2010; Cazorla et al., 2013; Liu et al., 2018), but in frame of the current capabilities in GRASP retrievals we could not advance with such analyses. Nevertheless, GRASP has revealed a small contribution of aerosol absorption in total aerosol optical depth during SLOPE I and II field campaigns even for cases with relatively low AODs.

**[Figure 7]**

The large standard deviations and percentiles observed in Figure 7 for all aerosol optical properties agree with the variability of aerosol types deduced from Figure 6. The aerosol variability can be caused by the fact that the different air-masses reach the south-east of Spain. Usually, the air-masses in the study region that come from the Atlantic brings clean air, from North of Africa transporting mineral dust, or from the Mediterranean transporting anthropogenic particles (e.g., Perez-Ramirez et al., 2016). Another frequent source of aerosol particle are the biomass burning events near to the study region (Alados-Arboledas et al., 2011; Ortiz-Amezcua et al., 2017; Sicard et al., 2019). According to the warning system of natural aerosol episodes of MITECO (Spanish Ministry for Ecological Transition and Demographic Challenge, https://www.miteco.gob.es/es/calidad-y-evaluacion-ambiental/temas/, last access: 1 June 2020), around the 66% and 10% of the evaluated days with GRASP retrievals there were associated to North African intrusions and biomass burning events in the south-eastern of Spain, respectively.

### 4.2.2. Vertically-resolved

Figure 8 shows a statistical overview of the aerosol optical and microphysical properties profiles retrieved by GRASP: volume concentration, differentiating between fine and coarse mode, and for the aerosol optical properties the extinction, scattering and absorption coefficients plus SSA and LR, all at the reference wavelength of 532 nm. Additionally, we include the AAE and SAE computed between 355 and 1064 nm. As we commented in section 3.1., a total of 286 GRASP retrievals passed the filter imposed. For the statistical overview, we compare point by point the 60 altitudes log-spaced of each aerosol property profiles. The solid

black lines represent the medians and red dashed line the means. The shadowed area is the interquartile range and the black dashed lines represent 10th and 90th percentiles.

425       For aerosol microphysical properties (Figures 8a, b) we observe approximately a linear decay with altitude until they reach approximately zero at 4-5 km a.s.l.. The largest values are at the lowest altitudes (with average ~10 $\mu m^3/cm^3$). The VC$_F$ profile shows lower variability (smaller interquartile range) than VC$_C$ profile. The highest variability of coarse particles profile, being the 90th percentile with values between 40 and 60 $\mu m^3/cm^3$, is mainly caused by

430     the intrusion of desert dust particles during SLOPE I and II campaigns.

**[Figure 8]**

      The extinction, scattering and absorption coefficients profiles at 532 nm (Fig 8 c, d, e) show similar behaviour than VC profiles. These patterns of extinction coefficient profiles for long-term statistical analyses have been observed in Europe for previous studies using Raman

435     lidar data (e.g., Amiridis et al., 2005; Navas-Guzmán et al., 2013). The largest values for the particle extinction, scattering and absorption coefficients are observed for the altitudes below 2 km a.s.l. (40, 35 and 4 Mm$^{-1}$ for $\alpha$, $\sigma_{sca}$ and $\sigma_{abs}$, respectively). This behaviour of $\sigma_{sca}$ profile has been previously observed in other statistical lidar studies (e.g., Titos et al., 2019). The SSA profile at 532 nm decreases with values from 0.92 at lowest altitude to 0.86 at highest altitude,

440     and with interquartile range ~ 0.025 which is close to the uncertainties claimed for SSA retrievals using remote sensing techniques (e.g., Pérez-Ramírez et al., 2019). The combination of $\sigma_{abs}$ and SSA reveals that for the entire profile approximately 10% of total extinction corresponds to absorption. Thus, GRASP retrievals show the capability of this code to characterizing aerosol absorption coefficients with vertical resolution, being a step forward to

445     aerosol characterization.

      The profiles of intensive properties such as LR, AAE and SAE can provide information about predominance of different aerosol particle types. For LR at 532 nm (Figure 8g), a constant mean profile is observed with mean value of ~52 sr. LR at a given wavelength depends mainly both on chemical composition and particle shapes (Müller et al., 2007), which explains

450     the variability in the retrieved values for the different aerosol types with a strong contribution of mineral dust. The LR values obtained are very similar to the ones observed in other studies (e.g., Guerrero-Rascado et al., 2009; Navas-Guzmán et al., 2013a). For SAE (Figure 8h), which is more related to the predominant particle size, the highest value is found at the lowest altitude, suggesting larger predominance of fine particles closer to the surface This pattern agrees with

the assumption of higher anthropogenic aerosol loads at these altitudes which are dominated by fine mode particles. Furthermore, it agrees with the low mixture of transported mineral dust with anthropogenic pollution at altitudes above the atmospheric boundary layer top. Finally, AAE (Figure 8i), that is related with the chemical composition of the absorbing aerosol, follows a constant pattern with altitude with mean value of ~1.45 with a $10^{th}$ and $90^{th}$ percentiles equal to 1 and 2, respectively. These are the values typically found for Saharan mineral dust particles transport and their mixture with anthropogenic pollutants (Russell et al., 2010).

### 4.2.3. Special Events

During the SLOPE I and II campaigns were occurred two extreme events with $AOD_{440}$ ~ 1.0. The first one was a Saharan mineral dust outbreak (DD) in July 2016, and the second one was a biomass burning transport event (BB) in July 2017 with fires origin in Portugal. Figure 9 and 10 show the profiles of aerosol optical and microphysical properties for the DD and BB event, respectively. It is also included in these figures the time when retrievals were obtained, the AOD at each moment and the SNS measurements at available periods.

**[Figure 9]**

Figure 9 and 10 show that for the first day of each event ($20^{th}$ July 2016 and $26^{th}$ July 2017) decoupled aerosol layers were observed at ~ 4 km a.s.l., approximately. Such decoupled layers went gradually downward until they reached the altitude of ~ 2-3 km a.s.l. in the morning of the second day of the event, on $21^{st}$ July 2016 and $27^{th}$ July 2017, respectively. This phenomenon is known as entrainment event and it has been observed previously in Granada (Bravo-Aranda et al., 2015). These figures suggest that these entrainments affect both the intensive and extensive aerosol properties.

The analyses of microphysical properties profiles show important differences in volume concentration between these two extreme events. For DD event, coarse particles predominate with $VC_C$ between 200 and 300 $\mu m^3/cm^3$ on the aerosol layer, while for the BB event, the $VC_C$ is very low (~10 $\mu m^3/cm^3$) and fine particles predominate with maximum values between 60 and 105 $\mu m^3/cm^3$. In general, GRASP $VC_F$ overestimate SNS measurements with differences below 10 $\mu m^3/cm^3$, whereas GRASP $VC_C$ is similar to SNS measurements for values around 55 $\mu m^3/cm^3$ as shown in the Section 4.1.1.. However, for higher values of $VC_C$, GRASP overestimates the SNS data with differences between 10 and 20 $\mu m^3/cm^3$ as shown in Benavent et al. (2019).

For extensive optical properties, the $\sigma_{sca}$ profiles at 532 nm show similar values between both events, with values between 200 and 400 Mm$^{-1}$. However, for $\sigma_{abs}$ there are significant differences between both events, being observed larger values during the BB event probably because the presence of organic and black carbon particles. Nevertheless, we remark that $\sigma_{abs}$ is not negligible as expected for mineral dust particles (e.g., Valenzuela et al., 2012). These findings are supported from SSA profiles that shows lower SSA values for biomass burning (mean values ~0.83), and higher for dust events (mean values around 0.93).

Finally, Figures 9 and 10 also show the profiles obtained for intensive properties such as SAE and AAE, computed from GRASP retrievals (spectral range 355-1064 nm). The analyses of these variables can provide an indication of aerosol types. On 20th and 21st July 2016, the SAE values lower than 0.5 corroborate the predominance of coarse particles for mineral dust particles (Bergstrom et al., 2007), and the AAE values, ranging from 1.5 to 2.1, suggest a mixture of mineral dust and absorbing particles of anthropogenic origin (e.g., Giles et al., 2011; Valenzuela et al., 2015). During the BB event, the SAE values are around 2, indicating a scattering dominated by submicron particles, and the AAE values between 1.1 and 1.45 suggest the presence of carbonaceous particles (Giles et al., 2012). Nevertheless, further advancement in the interpretation of aerosol chemical composition is challenging now, while new development aiming on characterization of aerosol compositions are being included into GRASP (Li et al., 2019, 2020) and to be explored in the future.

## 5. Conclusions

In this study, we presented an overview of aerosol optical and microphysical properties retrieved with GRASP code during SLOPE I and II field campaigns. The measurements from lidar and sun-sky photometer performed on May, June and July 2016 and 2017 were used as input data in GRASP to retrieve these aerosol properties.

The in-situ measurements performed at Sierra Nevada Station during SLOPE I and II campaigns, and the airborne measurement gathered during special periods on both campaigns allowed the assessment of aerosol properties retrieved by GRASP code at 2.5 km a.s.l. and for the whole profile, respectively. The volume concentration comparison shows better agreement for coarse mode (R=0.83) than for fine and total modes. The range of values for fine mode is small due to the few cases (15 % of cases) with predominating fine particles, therefore, we cannot conclude the agreement of GRASP retrievals and in-situ measurements for fine mode. For the scattering and absorption coefficients, the differences between GRASP data at 2.5 km

a.s.l. and in-situ measurements are lowest for longest wavelengths, with differences of $11 \pm 17$ Mm$^{-1}$ at 450 nm and $2 \pm 6$ Mm$^{-1}$ at 370 nm for $\sigma_{sca}$ and $\sigma_{abs}$, respectively. The agreement between GRASP and in-situ measurements at SNS is solid for both scattering and absorption coefficients. In general, GRASP somewhat overestimates the in-situ data at 2.5 km a.s.l.. These differences ($14 \pm 10$ and $1.2 \pm 1.2$ Mm$^{-1}$ $\sigma_{sca}$ and $\sigma_{abs}$, respectively) are also observed in the whole profile when comparing GRASP retrievals and the airborne measurements performed on 15$^{th}$, 17$^{th}$ and 18$^{th}$ June 2016 and 21$^{st}$, 23$^{rd}$ and 24$^{th}$ June 2017.

The statistical analysis of SLOPE I and II campaigns show the values of aerosol optical depth (AOD$_{440}$ = $0.22 \pm 0.18$) and Ångström exponent (AE$_{440–870}$ = $0.8 \pm 0.4$) that are typical of those months in Granada. The large variety of aerosol properties values denotes a large variability of aerosol loads and types with a desert mineral dust predominance associated with North African intrusions in the south-eastern of Spain. The statistical overview of the volume concentration profiles shows a decay of the properties with the altitude, reaching approximately zero at 4-5 km a.s.l.. The coarse mode shows the highest variability being the 90$^{th}$ percentile with values between 40 and 60 $\mu m^3/cm^3$. The largest value for the absorption coefficient is observed at the lowest altitudes (4 Mm$^{-1}$). Finally, two extreme events (AOD$_{440}$ >1.0) were studied: Saharan desert dust intrusion and biomass burning from Portugal fires in July 2016 and 2017, respectively. The study of these events shows the high capabilities of GRASP to retrieve volume concentration profiles in both fine and coarse mode and potentially interesting capability of the algorithm to derive the profiles of the single scattering albedo and absorption coefficients for different types and sizes of atmospheric aerosols.

*Data availability.* The GRASP inversion algorithm software used in this work is free and publicly available at http://www.grasp-open.com (last access: 1 April 2020). Lidar and in-situ data are available from the authors upon request. Sun–sky photometer data are accessible on the AERONET website (http://aeronet.gsfc.nasa.gov/, last access: 1 April 2020).

*Author contributions.* The conceptualization was done by JABO and LAA. JABO performed the GRASP retrievals, analysed the data and wrote the manuscript. RR helped to perform GRASP retrievals. JACV and HL operated and processed the in-situ measurement at Sierra Nevada Station. GT, NP and AA performed the installation of the instrumentation on-board the aircraft and operated the instruments during the flights. AC processed the airborne in-situ

data. The lidar data acquisition was performed by JABO, GdAM, JLGR, POA, RR, and AEBV. MH and OD provided feedback on the GRASP algorithm. The formal analysis, investigation, writing of the original draft, preparation, review of the writing and editing were performed by JABO, JACV, RR, DPR, HL and MJGM. The project administration, funding acquisition and design of SLOPE I and II campaigns were done by FJOR and LAA. Coordination of the campaign has been responsibility of LAA. All authors provided comments on the manuscript and helped with paper correction.

*Competing interests.* The authors declare that they have no conflict of interest.

*Acknowledgements.* Jose Antonio Benavent-Oltra is funded by the University of Granada through "Plan Propio. Programa 7, Convocatoria 2019". Roberto Román is funded by MINECO under the postdoctoral programme Juan de la Cierva-Incorporación (IJCI2016-30007). Juan Andrés Casquero-Vera is funded by MINECO under the predoctoral programme FPI (BES-2017-080015). Maria J. Granados-Muñoz project has received funding from the European Union's Horizon 2020 research and innovation programme under the Marie Skłodowska-Curie grant agreement No 796539. Oleg Dubovik was supported by the Labex CaPPA project, which is funded by the French National Research Agency under contract "ANR-11-LABX0005-01". The authors thankfully acknowledge the FEDER programme for the instrumentation used in this work, the University of Granada, which supported this study through the excellence units programme, and the Sierra Nevada National Park. We also thank Dr. Grisa Monick who provided the Aethalometer AVIO AE-33 installed on the aircraft. The work is related to activities within the COST Action CA18235 PROBE (PROfiling the atmospheric Boundary layer at European scale). Thanks to AERONET and ACTRIS/AERONET-Europe for the scientific and technical support. Finally, the authors would like to acknowledge the use of the GRASP inversion algorithm software (http://www.grasp-open.com, last access: 1 April 2020) in this work.

*Financial support.* This research has been supported by the Spanish Ministry of Economy and Competitiveness (projects CMT2015-66742-R, CGL2016-81092- R, CGL2017-85344-R, RTI2018-097864-B-I00 and CGL2017- 90884-REDT), by by the Andalusia Regional Government through project P18-RT-3820, and by the Marie Skłodowska-Curie Research Innovation and Staff Exchange (RISE) GRASP-ACE (grant no. 778349) project. The authors

thankfully acknowledge the University of Granada that supported this study through the Excellence Units Program

585 **References**

Aladas-Arboledas, L., Muller, D., Guerrero-Rascado, J. L., Navas-Guzman, F., Pérez-Ramírez, D., and Olmo, F. J.: Optical and microphysical properties of fresh biomass burning aerosol retrieved by Raman lidar, and star- and sun-photometry, Geophys. Res. Lett., 38, L01807, https://doi.org/10.1029/2010GL045999, 2011.

590 Amiridis, V., Balis, D. S., Kazadzis, S., Bais, A., Giannakaki, E., Papayannis, A., and Zerefos, C.: Four-year aerosol observations with a Raman lidar at Thessaloniki, Greece, in the framework of European Aerosol Research Lidar Network (EARLINET), J. Geophys. Res., 110, D21203, https://doi.org/10.1029/2005JD006190, 2005.

Anderson, TL., and Ogren, J. A.: Determining aerosol radiative properties using the TSI 3563 integrating nephelometer, Aerosol Sci. Technol., 29, 57–69, 1998.

595 Ansmann, A., Riebesell, M., Wandinger, U., Weitkamp, C., Voss, E., Lahmann, W., and Michaelis, W.: Combined Raman elastic backscatter LIDAR vertical profiling of moisture, aerosol extinction, backscatter and LIDAR ratio, Appl. Phys. B, 55, 18–28, 1992.

Barreto, Á., Cuevas, E., Granados-Muñoz, M. J., Aladas-Arboledas, L., Romero, P. M., Gröbner, J., Kouremeti, N., Almansa, A. F., Stone, T., Toledano, C., Román, R., Sorokin, M., Holben, B., Canini, M., and Yela, M.: 600 The new sun-skylunar Cimel CE318-T multiband photometer – a comprehensive performance evaluation, Atmos. Meas. Tech., 9, 631–654, https://doi.org/10.5194/amt-9-631-2016, 2016.

Barreto, Á., Román, R., Cuevas, E., Pérez-Ramírez, D., J. Berjón, A., Kouremeti, N., Kazadzis, S., Gröbner, J., Mazzola, M., Toledano, C., Benavent-Oltra, J. A., Doppler, L., Juryšek, J., Almansa, A. F., Victori, S., Maupin, F., Guirado-Fuentes, C., González, R., Vitale, V., Goloub, P., Blarel, L., Aladas-Arboledas, L., 605 Woolliams, E., Greenwell, C., Taylor, S., Antuña, J. C., and Yela, M.: Evaluation of night-time aerosols measurements and lunar irradiance models in the frame of the first multi-instrument nocturnal intercomparison campaign , Atmos. Environ., 202, 190-211, https://doi.org/10.1016/j.atmosenv.2019.01.006, 2019.

Bedoya-Velásquez, A. E., Navas-Guzmán, F., Granados-Muñoz, M. J., Titos, G., Román, R., Casquero-Vera, J. A., Ortiz-Amezcua, P., Benavent-Oltra, J. A., de Arruda Moreira, G., Montilla-Rosero, E., Hoyos, C. D., 610 Artiñano, B., Coz, E., Olmo-Reyes, F. J., Aladas-Arboledas, L., and Guerrero-Rascado, J. L.: Hygroscopic growth study in the framework of EARLINET during the SLOPE I campaign: synergy of remote sensing and in situ instrumentation, Atmos. Chem. Phys., 18, 7001-7017, https://doi.org/10.5194/acp-18-7001-2018, 2018.

Bedoya-Velásquez, A.E., Navas-Guzmán, F., de Arruda Moreira, G., Román, R., Cazorla, A., Ortiz-Amezcua, P., Benavent-Oltra, J.A., Aladas-Arboledas, L., Olmo-Reyes, F.J., Foyo-Moreno, I., Montilla-Rosero, E., Hoyos, 615 C.D., Guerrero-Rascado, J.L. Seasonal analysis of the atmosphere during five years by using microwave radiometry over a mid-latitude site. Atmospheric Research, 218, pp. 78-89, https://doi.org/10.1016/j.atmosres.2018.11.014, 2019.

Benavent-Oltra, J. A., R. Román, M. J. Granados-Muñoz, D. Pérez-Ramírez, P. Ortiz-Amezcua, C. Denjean, A. Lopatin, H. Lyamani, B. Torres, J. L. Guerrero-Rascado, D. Fuertes, O. Dubovik, A. Chaikovsky, F. J. Olmo, 620 M. Mallet, and L. Aladas-Arboledas: Comparative assessment of GRASP algorithm for a dust event over Granada (Spain) during ChArMEx-ADRIMED 2013 campaign, Atmos. Meas. Tech., 10, 4439–4457, https://doi.org/10.5194/amt-10-4439-2017, 2017.

Benavent-Oltra, J. A., Román, R., Casquero-Vera, J. A., Pérez-Ramírez, D., Lyamani, H., Ortiz-Amezcua, P., Bedoya-Velásquez, A. E., de Arruda Moreira, G., Barreto, Á., Lopatin, A., Fuertes, D., Herrera, M., Torres, 625 B., Dubovik, O., Guerrero-Rascado, J. L., Goloub, P., Olmo-Reyes, F. J., and Aladas-Arboledas, L.: Different strategies to retrieve aerosol properties at night-time with the GRASP algorithm, Atmos. Chem. Phys., 19, 14149–14171, https://doi.org/10.5194/acp-19-14149-2019, 2019.

Bergstrom, R.W., Pilewskie, P., Russell, P. B., Redemann, J., Bond, T. C., Quinn, P. K., and Sierau, B.: Spectral absorption properties of atmospheric aerosols, Atmos. Chem. Phys., 7, 5937-5943, 630 https://doi.org/10.5194/acp-7-5937-2007, 2007.

Böckmann, C.: Hybrid regularization method for the ill-posed inversion of multiwavelength lidar data to determine aerosol size distributions, Appl. Optics, 40, 1329-1342, 2001.

Bravo-Aranda, J. A., Titos, G., Granados-Muñoz, M. J., Guerrero-Rascado, J. L., Navas-Guzmán, F., Valenzuela, A., Lyamani, H., Olmo, F. J., Andrey, J., and Aladas-Arboledas, L.: Study of mineral dust entrainment in the

635      planetary boundary layer by lidar depolarisation technique, Tellus B, 67, 26180, doi:10.3402/tellusb.v67.26180, 2015.

Cariñanos, P., Foyo-Moreno, I., Alados, I., Guerrero-Rascado, J.L., Ruiz-Peñuela, S., Titos, G., Cazorla, A., Alados-Arboledas, L. and Díaz de la Guardia, C. Bioaerosols in urban environments: Trends and interactions with pollutants and meteorological variables based on quasi-climatological series, Journal of Environmental
640      Management, 282, 111963, https://doi.org/10.1016/j.jenvman.2021.111963, 2021.

Casquero-Vera, J. A., Lyamani, H., Dada, L., Hakala, S., Paasonen, P., Román, R., Fraile, R., Petäjä, T., Olmo-Reyes, F. J., and Alados-Arboledas, L.: New particle formation at urban and high-altitude remote sites in the south-eastern Iberian Peninsula, Atmos. Chem. Phys., 20, 14253–14271, https://doi.org/10.5194/acp-20-14253-2020, 2020.

645 Casquero-Vera, J. A., Lyamani, H., Titos, G., Minguillón, M. C., Dada, L., Alastuey, A., Querol X., Petäjä T., Olmo F.J., Alados-Arboledas L.: Quantifying traffic, biomass burning and secondary source contributions to atmospheric particle number concentrations at urban and suburban sites. Science of the Total Environment, 768, https://doi.org/10.1016/j.scitotenv.2021.145282, 2021.

Cazorla, A., Bahadur, R., Suski, K. J., Cahill, J. F., Chand, D., Schmid, B., Ramanathan, V., and Prather, K. A.:
650      Relating aerosol absorption due to soot, organic carbon, and dust to emission sources determined from in-situ chemical measurements, Atmos. Chem. Phys., 13, 9337–9350, https://doi.org/10.5194/acp-13-9337-2013, 2013.

Caumont, O., Cimini, D., Löhnert, U., Alados-Arboledas, L., Bleisch, R., Buffa, F., Ferrario, M. E., Haefele, A., Huet, T., Madonna, F., and Pace, G.: Assimilation of humidity and temperature observations retrieved from
655      ground-based microwave radiometers into a convective-scale NWP model, Q. J. Roy. Meteorol. Soc., 142, 2692–2704, https://doi.org/10.1002/qj.2860, 2016.

Chaikovsky, A., Dubovik, O., Goloub, P., Balashevich, N., Lopatsin, A., Karol, Y., Denisov, S. and Lapyonok, T.: Software package for the retrieval of aerosol microphysical properties in the vertical column using combined lidar/photometer data (test version), Technical Report, Minsk, Belarus, Institute of Physics, National
660      Academy of Sciences of Belarus, 2008.

Chaikovsky, A., Dubovik, O., Holben, B., Bril, A., Goloub, P., Tanré, D., Pappalardo, G., Wandinger, U., Chaikovskaya, L., Denisov, S., Grudo, J., Lopatin, A., Karol, Y., Lapyonok, T., Amiridis, V., Ansmann, A., Apituley, A., Allados-Arboledas, L., Binietoglou, I., Boselli, A., D'Amico, G., Freudenthaler, V., Giles, D., Granados-Muñoz, M. J., Kokkalis, P., Nicolae, D., Oshchepkov, S., Papayannis, A., Perrone, M. R.,
665      Pietruczuk, A., Rocadenbosch, F., Sicard, M., Slutsker, I., Talianu, C., De Tomasi, F., Tsekeri, A., Wagner, J., and Wang, X.: Lidar-Radiometer Inversion Code (LIRIC) for the retrieval of vertical aerosol properties from combined lidar/radiometer data: development and distribution in EARLINET, Atmos. Meas. Tech., 9, 1181-1205, https://doi.org/10.5194/amt-9-1181-2016, 2016.

Chen, C., Dubovik, O., Henze, D. K., Lapyonak, T., Chin, M., Ducos, F., Litvinov, P., Huang, X., and Li, L.:
670      Retrieval of desert dust and carbonaceous aerosol emissions over Africa from POLDER/PARASOL products generated by the GRASP algorithm, Atmos. Chem. Phys., 18, 12551-12580. https://doi.org/10.5194/acp-18-12551-2018, 2018.

Chen, C., Dubovik, O., Henze, D. K., Chin, M., Lapyonok, T., Schuster, G. L., Ducos, F., Fuertes, D., Litvinov, P., Li, L., Lopatin, A., Hu, Q., and Torres, B.: Constraining global aerosol emissions using
675      POLDER/PARASOL satellite remote sensing observations, Atmos. Chem. Phys., 19, 14585–14606, https://doi.org/10.5194/acp-19-14585-2019, 2019.

de Arruda Moreira, G., Guerrero-Rascado, J. L., Bravo-Aranda, J. A., Benavent-Oltra, J. A., Ortiz-Amezcua, P., Román, R., Bedoya-Velásquez, A. E., Landulfo, E., and Alados-Arboledas, L.: Study of the planetary boundary layer by microwave radiometer, elastic lidar and Doppler lidar estimations in Southern Iberian
680      Peninsula, Atmos. Res., 213, 185–195, https://doi.org/10.1016/j.atmosres.2018.06.007, 2018.

de Arruda Moreira, G., Guerrero-Rascado, J. L., Benavent-Oltra, J. A., Ortiz-Amezcua, P., Román, R., E. Bedoya-Velásquez, A., Bravo-Aranda, J. A., Olmo Reyes, F. J., Landulfo, E., and Alados-Arboledas, L.: Analyzing the turbulent planetary boundary layer by remote sensing systems: the Doppler wind lidar, aerosol elastic lidar and microwave radiometer, Atmos. Chem. Phys., 19, 1263-1280, https://doi.org/10.5194/acp-19-1263-2019,
685      2019.

del Águila, A., Sorribas, M., Lyamani, H., Titos, G., Olmo, F.J., Arruda-Moreira, G., Yela, M., Alados-Arboledas, L. Sources and physicochemical characteristics of submicron aerosols during three intensive campaigns in Granada (Spain), https://doi.org/10.1016/j.atmosres.2018.06.004, Atmospheric Research, 213, pp. 398-410, 2018.

690 Dubovik, O. and M. D. King, "A flexible inversion algorithm for retrieval of aerosol optical properties from Sun and sky radiance measurements", J. Geophys. Res., 105, 20,673-20,696, 2000.

Dubovik, O., Smirnov, A., Holben, B.N., King, M.D., Kaufman, Y., Eck, T.F., Slutsker, I.: Accuracy assessments of aerosol optical properties retrieved from AerosolRobotic Network (AERONET) Sun and sky radiance measurements. J. Geophys. Res.105, 9791–9806, 2000.

695 Dubovik, O., M. Herman, A. Holdak, T. Lapyonok, D. Tanré, J. L. Deuzé, F. Ducos, A. Sinyuk, and A. Lopatin, "Statistically optimized inversion algorithm for enhanced retrieval of aerosol properties from spectral multi-angle polarimetric satellite observations", Atmos. Meas. Tech., 4, 975-1018, 2011.

Dubovik, O., Lapyonok, T., Litvinov, P., Herman, M., Fuertes, D., Ducos, F., Lopatin, A., Chaikovsky, A., Torres, B., Derimian, Y., Huang, X., Lopatin, A., Chaikovsky, A., Aspetsberger, M., and Federspiel, C.: Grasp: a
700 versatile algorithm for characterizing the atmosphere. SPIE Newsroom, 25, 2014.

Dubovik, O., Li, Z., Mishchenko, M. I., Tanré, D., Karol, Y., Bojkov, B., Cairns, B., Diner, D. J., Espinosa, W. R., Goloub, P., Gu, X., Hasekamp, O., Hong, J., Hou, W., Knobelspiess, K. D., Landgraf, J., Li, L., Litvinov, P., Liu, Y., Lopatin, A., Marbach, T., Maring, H., Martins, V., Meijer, Y., Milinevsky, G., Mukai, S., Parol, F., Qiao, Y., Remer, L., Rietjens, J., Sano, I., Stammes, P., Stamnes, S., Sun, X., Tabary, P., Travis, L. D.,
705 Waquet, F., Xu, F., Yan, C., and Yin, D.: Polarimetric remote sensing of atmospheric aerosols: Instruments, methodologies, results, and perspectives, J. Quant. Spectrosc. Ra., 224, 474–511, https://doi.org/10.1016/j.jqsrt.2018.11.024, 2019.

Drinovec, L., Močnik, G., Zotter, P., Prévôt, A. S. H., Ruckstuhl, C., Coz, E., Rupakheti, M., Sciare, J., Müller, T., Wiedensohler, A., and Hansen, A. D. A.: The "dual-spot" Aethalometer: an improved measurement of
710 aerosol black carbon with real-time loading compensation, Atmos. Meas. Tech., 8, 1965–1979, https://doi.org/10.5194/amt-8-1965-2015, 2015.

Espinosa, W. R., Remer, L. A., Dubovik, O., Ziemba, L., Beyersdorf, A., Orozco, D., Schuster, G., Lapyonok, T., Fuertes, D., and Martins, J. V.: Retrievals of aerosol optical and microphysical properties from Imaging Polar Nephelometer scattering measurements, Atmos. Meas. Tech., 10, 811–824, https://doi.org/10.5194/amt-10-
715 811-2017, 2017.

Fernald, F. G., Herman, B. M., and Reagan, J. A.: Determination of aerosol height distributions by lidar, J. Appl. Meteorol., 11, 482–489, 1972.

Fernald, F. G.: Analysis of atmospheric lidar observations- Some comments, App. Optics, 23, 652–653, 1984.

Giles, D. M., Holben, B. N., Tripathi, S. N., Eck, T. F., Newcomb, W. W., Slutsker, I., Dickerson, R. R.,
720 Thompson, A. M., Mattoo, S., Wang, S., Singh, R. P., Sinyuk, A., and Schafer, J. S.: Aerosol properties over the Indo-Gangetic Plain: A mesoscale perspective from the TIGERZ experiment, J. Geophys. Res.-Atmos., 116. D18203, https://doi.org/10.1029/2011JD015809, 2011.

Giles, D. M., Holben, B. N., Eck, T. F., Sinyuk, A., Smirnov,A., Slutsker, I., Dickerson, R. R., Thompson, A. M., and Schafer, J. S.: An analysis of AERONET aerosol absorption properties and classifications representative
725 of aerosol source regions, J. Geophys. Res.-Atmos., 117, 127–135, https://doi.org/10.1029/2012JD018127, 2012.

Giles, D. M., Sinyuk, A., Sorokin, M. G., Schafer, J. S., Smirnov, A., Slutsker, I., Eck, T. F., Holben, B. N., Lewis, J. R., Campbell, J. R., Welton, E. J., Korkin, S. V., and Lyapustin, A. I.: Advancements in the Aerosol Robotic Network (AERONET) Version 3 database – automated near-real-time quality control algorithm with improved
730 cloud screening for Sun photometer aerosol optical depth (AOD) measurements, Atmos. Meas. Tech., 12, 169–209, https://doi.org/10.5194/amt-12-169-2019, 2019.

Granados-Muñoz, M. J., Sicard, M., Román, R., Benavent-Oltra, J. A., Barragán, R., Brogniez, G., Denjean, C., Mallet, M., Formenti, P., Torres, B., and Alados-Arboledas, L.: Impact of mineral dust on shortwave and longwave radiation: evaluation of different vertically resolved parameterizations in 1-D radiative transfer
735 computations , Atmos. Chem. Phys., 19, 523-542, https://doi.org/10.5194/acp-19-523-2019, 2019.

Granados-Muñoz, M.J., Benavent-Oltra, J.A., Pérez-Ramírez, D., Lyamani, H., Guerrero-Rascado, J.L., Bravo-Aranda, J.A., Navas-Guzmán, F., Valenzuela, A., Olmo, F.J., Alados-Arboledas, L. Evaluation of LIRIC algorithm performance using independent sun-sky photometer data at two altitude levels Remote Sensing, 12 (5), art. no. 842, https://www.mdpi.com/2072-4292/12/5/842, 2020.

740 Guerrero-Rascado, J. L., Ruiz, B., and Alados Arboledas, L.: Multispectral Lidar characterization of the vertical structure of Saharan dust aerosol over southern Spain, Atmos. Environ., 42, 2668– 2681, https://doi.org/10.1016/j.atmosenv.2007.12.062, 2008.

Guerrero-Rascado, J. L., Olmo, F. J., Avilés-Rodríguez, I., Navas-Guzmán, F., Pérez-Ramírez, D., Lyamani, H., and Alados Arboledas, L.: Extreme Saharan dust event over the southern Iberian Peninsula in september 2007:
745 active and passive remote sensing from surface and satellite, Atmos. Chem. Phys., 9, 8453-8469, doi:10.5194/acp-9-8453-2009, 2009.

Herreras, M., Román, R., Cazorla, A., Toledano, C., Lyamani, H., Torres, B., Cachorro, V.E., Olmo, F.J., Alados-Arboledas, L. and de Frutos., A.M.: Evaluation of retrieved aerosol extinction profiles using as reference the aerosol optical depth differences between various heights, Atmospheric Research, 230, https://doi.org/10.1016/j.atmosres.2019.104625, 2019.

Holben, B. N., Eck, T. F., Slutsker, I., Tanre, D., Buis, J. P., Setzer, A., Vermote, E., Reagan, J. A., Kaufman, Y. J., Nakajima, T., Lavenu, F., Jankowiak, I., and Smirnov, A.: AERONET-a federated instrument network a data archive for aerosol characterization, Remote Sens. Environ., 66, 1–16, 1998.

Horvath, H., Alados Arboledas, L., and Olmo Reyes, F. J.: Angular scattering of the Sahara dust aerosol, Atmos. Chem. Phys., 18, 17735-17744, https://doi.org/10.5194/acp-18-17735-2018, 2018.

IPCC: Contribution of Working Group I to the Fifth Assessment Report of the Intergovernmental Panel on Climate Change, Summary for Policymakers in Climate Change, Stocker, Cambridge University Press, Cambridgen, 2013.

Klett, J. D.: Stable analytical inversion solution for processing lidar returns, Appl. Optics, 20, 211–220, 1981.

Li., L., O. Dubovik, Y. Derimian, G. L. Schuster, T. Lapyonok, P. Litvinov, F. Ducos, D. Fuertes, C. Chen, Z. Li, A. Lopatin, B. Torres and H. Che, "Retrieval of aerosol components directly from satellite and ground-based measurements", Atmos. Chem. Phys. 19, 13409–13443, https://doi.org/10.5194/acp-19-13409-2019, 2019.

Li, L., H. Che, Y. Derimian, O. Dubovik, G. Schuster, C. Chen, Q. Lid, Y. Wang, B. Guo and X. Zhang, "Retrievals of fine mode light-absorbing carbonaceous aerosols from POLDER/PARASOL observations over East and South Asia", Remote Sens. Environ., 247, Article Number: 111913, DOI: 10.1016/j.rse.2020.111913, 2020.

Liu, D., Taylor, J. W., Crosier, J., Marsden, N., Bower, K. N., Lloyd, G., Ryder, C. L., Brooke, J. K., Cotton, R., Marenco, F., Blyth, A., Cui, Z., Estelles, V., Gallagher, M., Coe, H. and Choularton, T. W.: Aircraft and ground measurements of dust aerosols over the west African coast in summer 2015 during ICE-D and AER-D, Atmos. Chem. Phys., 18(5), 3817–3838, doi:10.5194/acp-18-3817-2018, 2018.

Lopatin, A., Dubovik, O., Chaikovsky, A., Goloub, P., Lapyonok, T., Tanré, D., and Litvinov, P.: Enhancement of aerosol characterization using synergy of lidar and sun-photometer coincident observations: the GARRLiC algorithm, Atmos. Meas. Tech., 6, 2065–2088, https://doi.org/10.5194/amt-6-2065-2013, 2013.

Lyamani, H., Olmo, F. J., and Alados-Arboledas, L.: Physical and optical properties of aerosols over an urban location in Spain: seasonal and diurnal variability, Atmos. Chem. Phys., 10, 239-254, https://doi.org/10.5194/acp-10-239-2010, 2010.

Mallet, M., Dulac, F., Formenti, P., Nabat, P., Sciare, J., Roberts, G., Pelon, J., Ancellet, G., Tanré, D., Parol, F., Denjean, C., Brogniez, G., di Sarra, A., Alados-Arboledas, L., Arndt, J., Auriol, F., Blarel, L., Bourrianne, T., Chazette, P., Chevaillier, S., Claeys, M., D'Anna, B., Derimian, Y., Desboeufs, K., Di Iorio, T., Doussin, J.-F., Durand, P., Féron, A., Freney, E., Gaimoz, C., Goloub, P., Gómez-Amo, J. L., Granados-Muñoz, M. J., Grand, N., Hamonou, E., Jankowiak, I., Jeannot, M., Léon, J.-F., Maillé, M., Mailler, S., Meloni, D., Menut, L., Momboisse, G., Nicolas, J., Podvin, T., Pont, V., Rea, G., Renard, J.-B., Roblou, L., Schepanski, K., Schwarzenboeck, A., Sellegri, K., Sicard, M., Solmon, F., Somot, S., Torres, B., Totems, J., Triquet, S., Verdier, N., Verwaerde, C., Waquet, F., Wenger, J., and Zapf, P.: Overview of the Chemistry-Aerosol Mediterranean Experiment/Aerosol Direct Radiative Forcing on the Mediterranean Climate (ChArMEx/ADRIMED) summer 2013 campaign, Atmos. Chem. Phys., 16, 455–504, https://doi.org/10.5194/acp-16-455-2016, 2016.

Müller, D., Wandinger, U., and Ansmann, A.: Microphysical particle parameters from extinction and backscatter lidar data by inversion with regularization: simulation, Appl. Opt. 38, 2358-2368, 1999.

Müller, D., Ansmann, A., Mattis, I., Tesche, M., Wandinger, U., Althausen, D., and Pisani, G.: Aerosol-type-dependent lidar ratios observed with Raman lidar, J. Geophys. Res.-Atmos., 112, D16202, doi:10.1029/2006jd008292, 2007.

Müller, T., Laborde, M., Kassell, G., and Wiedensohler, A.: Design and performance of a three-wavelength LED-based total scatter and backscatter integrating nephelometer, Atmospheric Measurement Techniques, 4, 1291–1303, 2011.

Navas-Guzmán, F., Bravo-Aranda, J. A., Guerrero-Rascado, J. L., Granados-Muñoz, M. J., and Alados-Arboledas, L.: Statistical analysis of aerosol optical properties retrieved by Raman lidar over Southeastern Spain, Tellus B, 65, 21234, https://doi.org/10.3402/tellusb.v65i0.21234, 2013.

Navas-Guzmán, F., Fernández-Gálvez, J., Granados-Muñoz, M. J., Guerrero-Rascado, J. L., Bravo-Aranda, J. A., and Alados-Arboledas, L.: Tropospheric water vapour and relative humidity profiles from lidar and microwave radiometry, Atmos. Meas. Tech., 7, 1201–1211, https://doi.org/10.5194/amt-7-1201-2014, 2014.

Ortiz-Amezcua, P., Guerrero-Rascado, J. L., Granados-Muñoz, M. J., Benavent-Oltra, J. A., Böckmann, C., Samaras, S., Stachlewska, I. S., Janicka, Ł., Baars, H., Bohlmann, S., and Alados-Arboledas, L.: Microphysical characterization of long-range transported biomass burning particles from North America at three EARLINET stations, Atmos. Chem. Phys., 17, 5931–5946, https://doi.org/10.5194/acp-17-5931-2017, 2017.

Ortiz-Amezcua, P., Bedoya-Velásquez, A. E., Benavent-Oltra, J. A., Pérez-Ramírez, D., Veselovskii, I., Castro-Santiago, M., Bravo-Aranda, J.A., Guedes, A., Guerrero-Rascado, J. L., and Alados-Arboledas, L.: Implementation of UV rotational Raman channel to improve aerosol retrievals from multiwavelength lidar, Opt. Express 28, 8156-8168, https://doi.org/10.1364/OE.383441, 2020.

Pappalardo, G., Amodeo, A., Apituley, A., Comeron, A., Freudenthaler, V., Linné, H., Ansmann, A., Bösenberg, J., D'Amico, G., Mattis, I., Mona, L., Wandinger, U., Amiridis, V., Alados-Arboledas, L., Nicolae, D., and Wiegner, M.: EARLINET: towards an advanced sustainable European aerosol lidar network, Atmos. Meas. Tech., 7, 2389–2409, https://doi.org/10.5194/amt-7-2389-2014, 2014.

Pérez-Ramírez, D., Lyamani, H., Olmo, F. J., Whiteman, D. N., and Alados-Arboledas, L.: Columnar aerosol properties from sun-and-star photometry: statistical comparisons and day-to-night dynamic, Atmos. Chem. Phys., 12, 9719-9738, https://doi.org/10.5194/acp-12-9719-2012, 2012.

Pérez-Ramírez, D., Lyamani, H., Smirnov, A., O'Neill, N. T., Veselovskii, I., Whiteman, D. N., Olmo, F. J., Alados-Arboledas, L.: Statistical study of day and night hourly patterns of columnar aerosol properties using sun and star photometry, Proc. SPIE, 100001, 100010K, 2016.

Perez-Ramirez, D., Whiteman D. N., Veselovskii, I., Colarco, P., Korenski, M., and da Silva, A.: Retrievals of aerosol single scattering albedo by multiwavelength lidar measurements: Evaluations with NASA Langley HSRL-2 during discover-AQ field campaigns, Remote Sens. Environ., 222, 144–164, 2019.

Román, R., Cazorla, A., Toledano, C., Olmo, F.J., Cachorro, V.E., de Frutos, A., Alados-Arboledas, L.: Cloud cover detection combining high dynamic range sky images and ceilometer measurements. Atmos. Res. 196, 224–236, https://doi.org/10.1016/j.atmosres.2017.06.006, 2017.

Román, R., J. A. Benavent-Oltra, J. A. Casquero-Vera, A. Lopatin, A. Cazorla, H. Lyamani, C. Denjean, D. Fuertes, D. Pérez-Ramírez, B. Torres, C. Toledano, O. Dubovik, V. E. Cachorro, Á. de Frutos, F. J. Olmo, and L. Alados-Arboledas: Retrieval of aerosol profiles combining sun photometer and ceilometer measurements in GRASP code, Atmospheric Research, 204, 161–177, https://doi.org/10.1016/j.atmosres.2018.01.021, 2018.

Román, R., González, R., Toledano, C., Barreto, Á., Pérez-Ramírez, D., Benavent-Oltra, J. A., Olmo, F. J., Cachorro, V. E., Alados-Arboledas, L., and de Frutos, Á. M.: Correction of a lunar-irradiance model for aerosol optical depth retrieval and comparison with a star photometer, Atmos. Meas. Tech., 13, 6293–6310, https://doi.org/10.5194/amt-13-6293-2020, 2020.

Rose, T., Crewell, S., Löhnert, U., and Simmer, C.: A network suitable microwave radiometer for operational monitoring of the cloudy atmosphere, Atmos. Res., 75, 183–200, 2005.

Russell, P. B., Bergstrom, R. W., Shinozuka, Y., Clarke, A. D., DeCarlo, P. F., Jimenez, J. L., Livingston, J. M., Redemann, J., Dubovik, O., and Strawa, A.: Absorption Angstrom Exponent in AERONET and related data as an indicator of aerosol composition, Atmos. Chem. Phys., 10, 1155–1169, https://doi.org/10.5194/acp-10-1155-2010, 2010.

Shin, S.-K., Tesche, M., Kim, K., Kezoudi, M., Tatarov, B., Müller, D., and Noh, Y.: On the spectral depolarisation and lidar ratio of mineral dust provided in the AERONET version 3 inversion product, Atmos. Chem. Phys., 18, 12735–12746, https://doi.org/10.5194/acp-18-12735-2018, 2018.

Sicard, M., Granados-Muñoz, M.J., Alados-Arboledas, L., Barragán, R., Bedoya-Velásquez, A.E., Benavent-Oltra, J.A., Bortoli, D., Comerón, A., Córdoba-Jabonero, C., Costa, M.J., del Águila, A., Fernández, A.J., Guerrero-Rascado, J.L., Jorba, O., Molero, F., Muñoz-Porcar, C., Ortiz-Amezcua, P., Papagiannopoulos, N., Potes, M., Pujadas, M., Rocadenbosch, F., Rodríguez-Gómez, A., Román, R., Salgado, R., Salgueiro, V., Sola, Y., Yela, M.: Ground/space, passive/active remote sensing observations coupled with particle dispersion modelling to understand the inter-continental transport of wildfire smoke plumes. Remote Sensing of Environment. 232. https://doi.org/10.1016/j.rse.2019.111294, 2019.

Sinyuk, A., Holben, B. N., Eck, T. F., Giles, D. M., Slutsker, I., Korkin, S., Schafer, J. S., Smirnov, A., Sorokin, M., and Lyapustin, A.: The AERONET Version 3 aerosol retrieval algorithm, associated uncertainties and comparisons to Version 2, Atmos. Meas. Tech., 13, 3375–3411, https://doi.org/10.5194/amt-13-3375-2020, 2020.

Sorribas, M., Olmo, F.J., Quirantes, A., Lyamani, H., Gil-Ojeda, M., Alados-Arboledas, L., Horvath, H.: Role of spheroidal particles in closure studies for aerosol microphysical-optical properties. Quarterly Journal of the Royal Meteorological Society. 141 - 692, pp. 2700 -2707, 2015.

Tanré, D., Haywood, J., Pelon, J., Léon, J. F., Chatenet, B., Formenti, P., Francis, P., Goloub, P., Highwood, E. J., Myhre, G.: Measurements and modeling of the Saharan dust radiative impact: overview of the Saharan Dust Experiment (SHADE). J. Geophys. Res. 108, doi:10.1029/2002JD003273, 2003.

860   Titos, G., Ealo, M., Román, R., Cazorla, A., Sola, Y., Dubovik, O., Alastuey, A., and Pandolfi, M.: Retrieval of aerosol properties from ceilometer and photometer measurements: long-term evaluation with in situ data and statistical analysis at Montsec (southern Pyrenees), Atmos. Meas. Tech., 12, 3255–3267, https://doi.org/10.5194/amt-12-3255-2019, 2019.

Torres, B., Dubovik, O., Fuertes, D., Schuster, G., Cachorro, V. E., Lapyonok, T., Goloub, P., Blarel, L., Barreto, 865   A., Mallet, M., Toledano, C., and Tanré, D.: Advanced characterisation of aerosol size properties from measurements of spectral optical depth using the GRASP algorithm, Atmos. Meas. Tech., 10, 3743-3781, https://doi.org/10.5194/amt-10-3743-2017, 2017.

Tsekeri, A., Lopatin, A., Amiridis, V., Marinou, E., Igloffstein, J., Siomos, N., Solomos, S., Kokkalis, P., Engelmann, R., Baars, H., Gratsea, M., Raptis, P. I., Binietoglou, I., Mihalopoulos, N., Kalivitis, N., 870   Kouvarakis, G., Bartsotas, N., Kallos, G., Basart, S., Schuettemeyer, D., Wandinger, U., Ansmann, A., Chaikovsky, A. P., and Dubovik, O.: GARRLiC and LIRIC: strengths and limitations for the characterization of dust and marine particles along with their mixtures, Atmos. Meas. Tech., 10, 4995-5016, https://doi.org/10.5194/amt-10-4995-2017, 2017.

Turco, M., Jerez, S., Augusto, S., Tarín-Carrasco, P., Ratola, N., Jiménez-Guerrero, P. and Trigo R. M.: Climate 875   drivers of the 2017 devastating fires in Portugal. Sci Rep 9, 13886, https://doi.org/10.1038/s41598-019-50281-2, 2019.

Valenzuela, A., Olmo, F.J., Lyamani, H., Antón, M., Quirantes, A., Alados- Arboledas, L.: Analysis of the desert dust radiative properties over Granada using principal plane sky radiances and spheroids retrieval procedure. Atmos. Res. 104–105, 292–301, https://doi.org/10.1016/j.atmosres.2011.11.005, 2012.

880   Valenzuela, A., Olmo, F. J., Lyamani, H., Antón, M., Titos, G., Cazorla, A., and Alados-Arboledas, L.: Aerosol scattering and absorption Angström exponents as indicators of dust and dust-free days over Granada (Spain), Atmos Res., 154, 1–13, https://doi.org/10.1016/j.atmosres.2014.10.015, 2015.

Vandenbussche, S., Callewaert, S., Schepanski, K., and De Mazière, M.: North African mineral dust sources: new insights from a combined analysis based on 3D dust aerosol distributions, surface winds and ancillary soil 885   parameters, Atmos. Chem. Phys., 20, 15127–15146, https://doi.org/10.5194/acp-20-15127-2020, 2020.

Veselovskii, I., Kolgotin, A., Griaznov, V., Muller, D., Wandinger, U., Whiteman, D: Inversion with regularization for the retrieval of tropospheric aerosol parameters from multiwavelength lidar sounding. Applied Optics, 41, 3685-3699, 2002.

Veselovskii, I., Whiteman, D. N., Korenskiy, M., Suvorina, A., and Pérez-Ramírez, D.: Use of rotational Raman 890   measurements in multiwavelength aerosol lidar for evaluation of particle backscattering and extinction, Atmos. Meas. Tech., 8, 4111–4122, https://doi.org/10.5194/amt-8-4111-2015, 2015.

Veselovskii, I., Goloub, P., Podvin, T., Bovchaliuk, V., Derimian, Y., Augustin, P., Fourmentin, M., Tanre, D., Korenskiy, M., Whiteman, D. N., Diallo, A., Ndiaye, T., Kolgotin, A., and Dubovik, O.: Retrieval of optical and physical properties of African dust from multiwavelength Raman lidar measurements during the 895   SHADOW campaign in Senegal, Atmos. Chem. Phys., 16, 7013–7028, https://doi.org/10.5194/acp-16-7013-2016, 2016.

Whiteman, D. N., Melfi, S. H., and Ferrare, R. A.: Raman lidar system for the measurement of water vapor and aerosols in the Earth's atmosphere, Appl. Optics, 31, 3068–3082, 1992.

Wiedensohler, A., Birmili, W., Nowak, A., Sonntag, A., Weinhold, K., Merkel, M., Wehner, B., Tuch, T., Pfeifer, 900   S., Fiebig, M., Fjäraa, A. M., Asmi, E., Sellegri, K., Depuy, R., Venzac, H., Villani, P., Laj, P., Aalto, P., Ogren, J. A., Swietlicki, E., Williams, P., Roldin, P., Quincey, P., Hüglin, C., Fierz-Schmidhauser, R., Gysel, M., Weingartner, E., Riccobono, F., Santos, S., Grüning, C., Faloon, K., Beddows, D., Harrison, R., Monahan, C., Jennings, S. G., O'Dowd, C. D., Marinoni, A., Horn, H.-G., Keck, L., Jiang, J., Scheckman, J., McMurry, P. H., Deng, Z., Zhao, C. S., Moerman, M., Henzing, B., de Leeuw, G., Löschau, G., and Bastian, S.: Mobility 905   particle size spectrometers: harmonization of technical standards and data structure to facilitate high quality long-term observations of atmospheric particle number size distributions, Atmos. Meas. Tech., 5, 657–685, https://doi.org/10.5194/amt-5-657-2012, 2012.

Wiedensohler, A., Wiesner, A., Weinhold, K., Birmili, W., Hermann, M., Merkel, M., Müller, T., Pfeifer, S., Schmidt, A., and Tuch, T.: Mobility particle size spectrometers: Calibration procedures and measurement 910   uncertainties, Aerosol Sci. Technol., 52, 146–164, 2018

Yus-Díez, J., Ealo, M., Pandolfi, M., Perez, N., Titos, G., Močnik, G., Querol, X., and Alastuey, A.: Aircraft vertical profiles during summertime regional and Saharan dust scenarios over the north-western Mediterranean

Basin: aerosol optical and physical properties, Atmos. Chem. Phys. Discuss., https://doi.org/10.5194/acp-2020-837, in review, 2020.

915

Table 1. Instruments deployed during SLOPE I and II campaigns at AGORA stations.

| Instrument | Location | Measurement variable | Wavelength (nm) / Nominal size range (µm) |
|---|---|---|---|
| Raman lidar system | UGR station | Elastic backscattered signal | 355, 532 and 1064 nm |
| Sun-sky photometer | UGR, CP and SNS stations | Aerosol optical depth and sky radiances | 440, 675, 870 and  1020 nm |
| Nephelometer        TSI 3563 | SNS station | Scattering coefficient | 450, 550, 700 nm |
| Nephelometer Aurora Ecotech | Aircraft | | 450, 525, 635 nm |
| Aethalometer AE-33 | SNS station | Absorption coefficient | 370, 470, 520, 590, 660, 880 and 950 nm |
| Aethalometer AVIO AE-33 | Aircraft | | |
| Scanning mobility particle sizer, TSI 3082 | SNS station | Aitken + accumulation mode conc. | 0.012 – 0.615 µm |
| Aerodynamic Particle Sizer, TSI 3321 | SNS station | Coarse mode conc. | 0.5 – 20 µm |
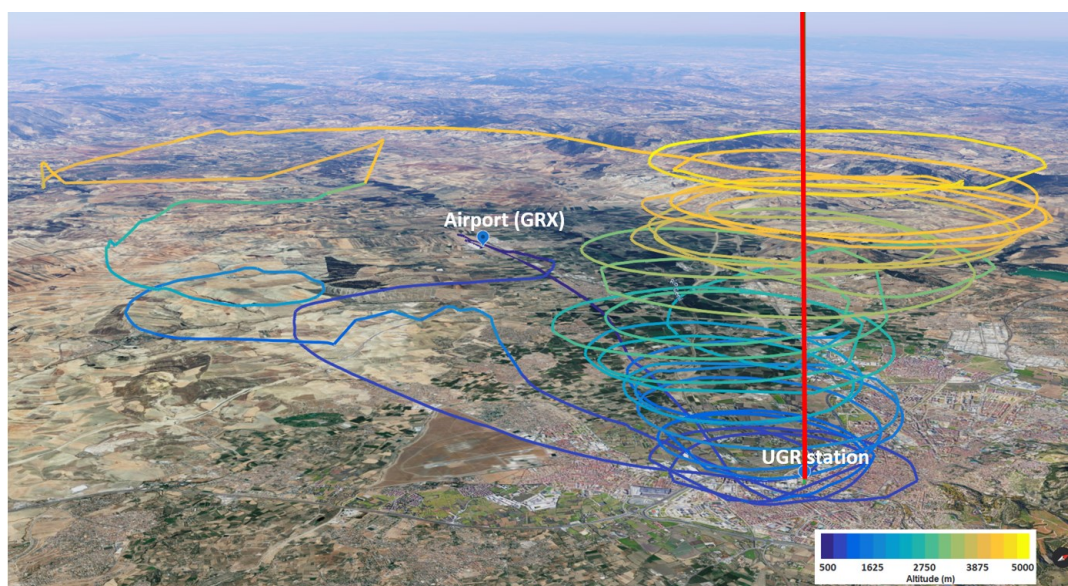
Figure 1.Map illustrating UGR station. The colored line indicates the trajectory of the aircraft and its altitude during the SLOPE II campaign.. The red line indicates the vertical of lidar measurements. © *Google Earth*

920
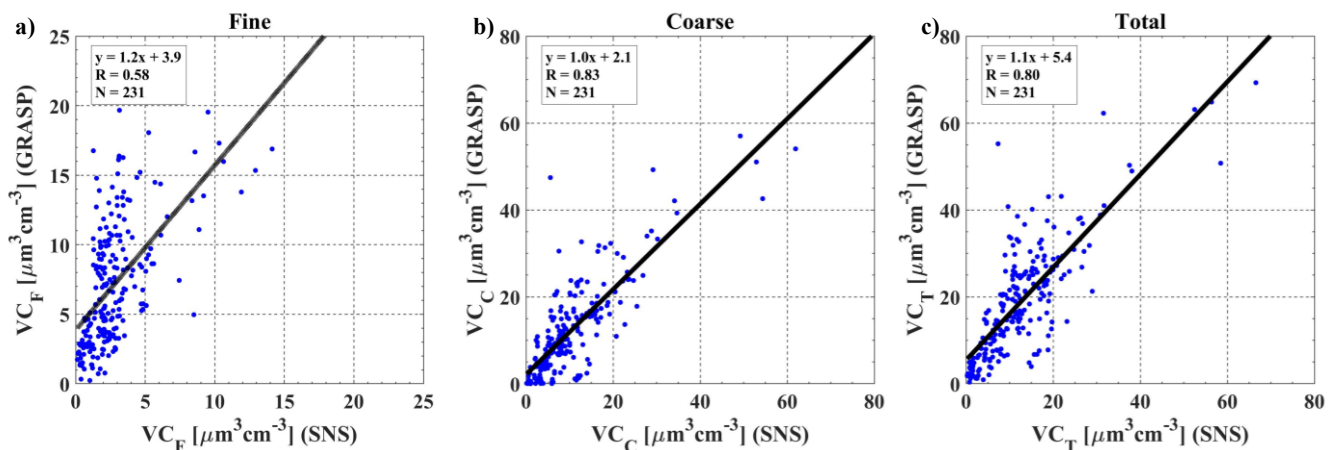
Figure 2. Volume concentration (VC) retrieved by GRASP at SNS height versus in-situ measurements at SNS for **(a)** fine, **(b)** coarse and **(c)** total modes.
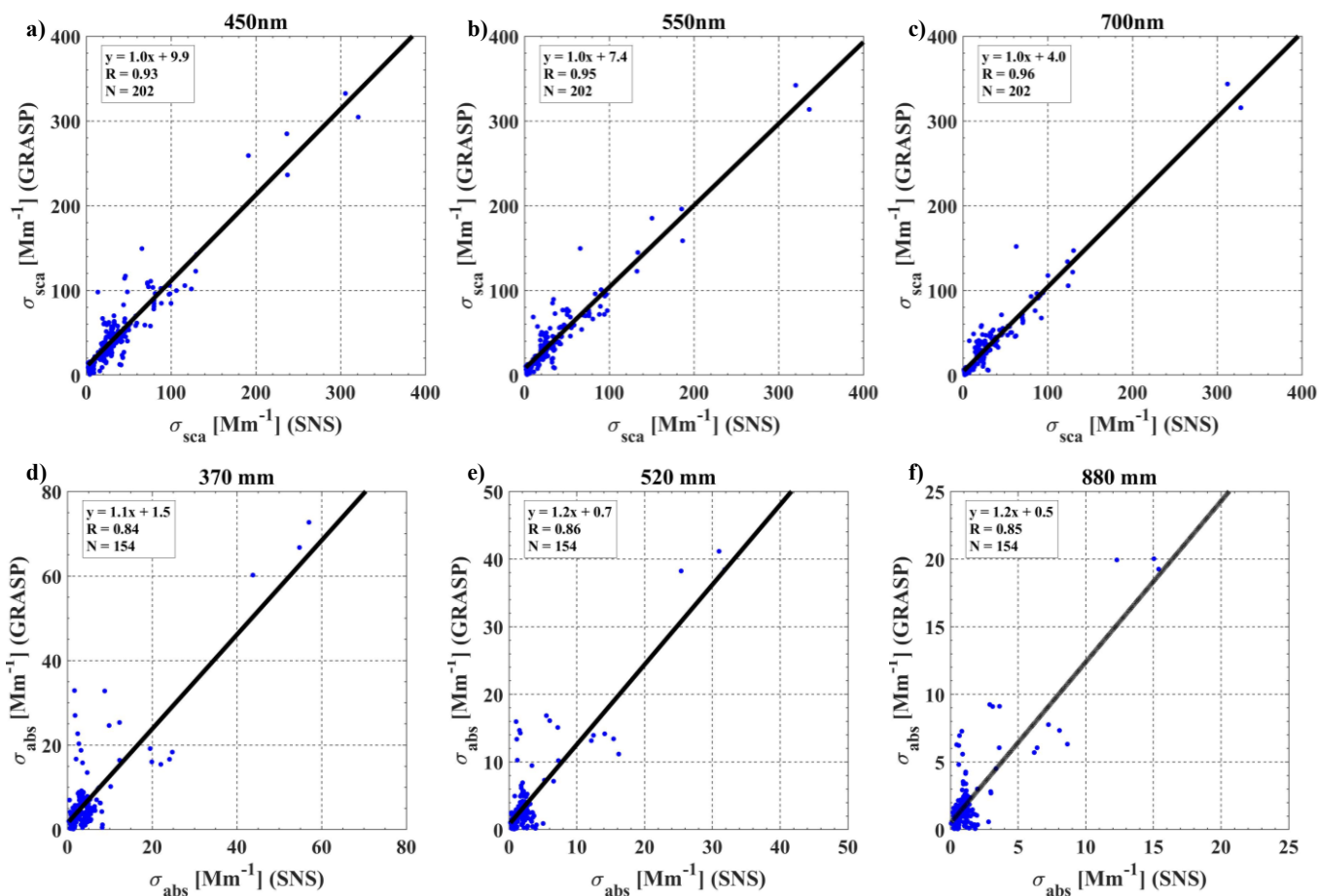
Figure 3. (**a, b, c**) Scattering ($\sigma_{sca}$) and (**d, e, f**) absorption ($\sigma_{abs}$) coefficients retrieved by GRASP at SNS height versus in-situ measurements at SNS.
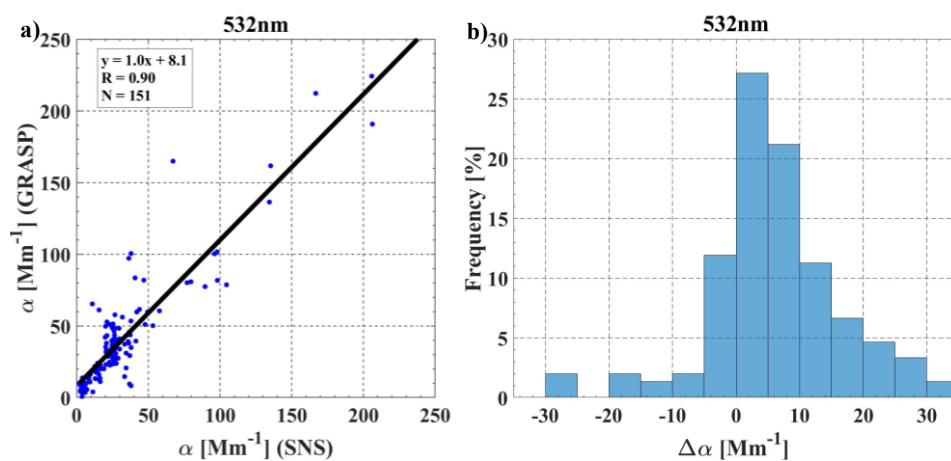
Figure 4. **(a)** Extinction ($\alpha$) coefficient retrieved by GRASP at SNS height versus the in-situ measurements at SNS and **(b)** the histogram of the absolute difference between GRASP and SNS in-situ measurements.
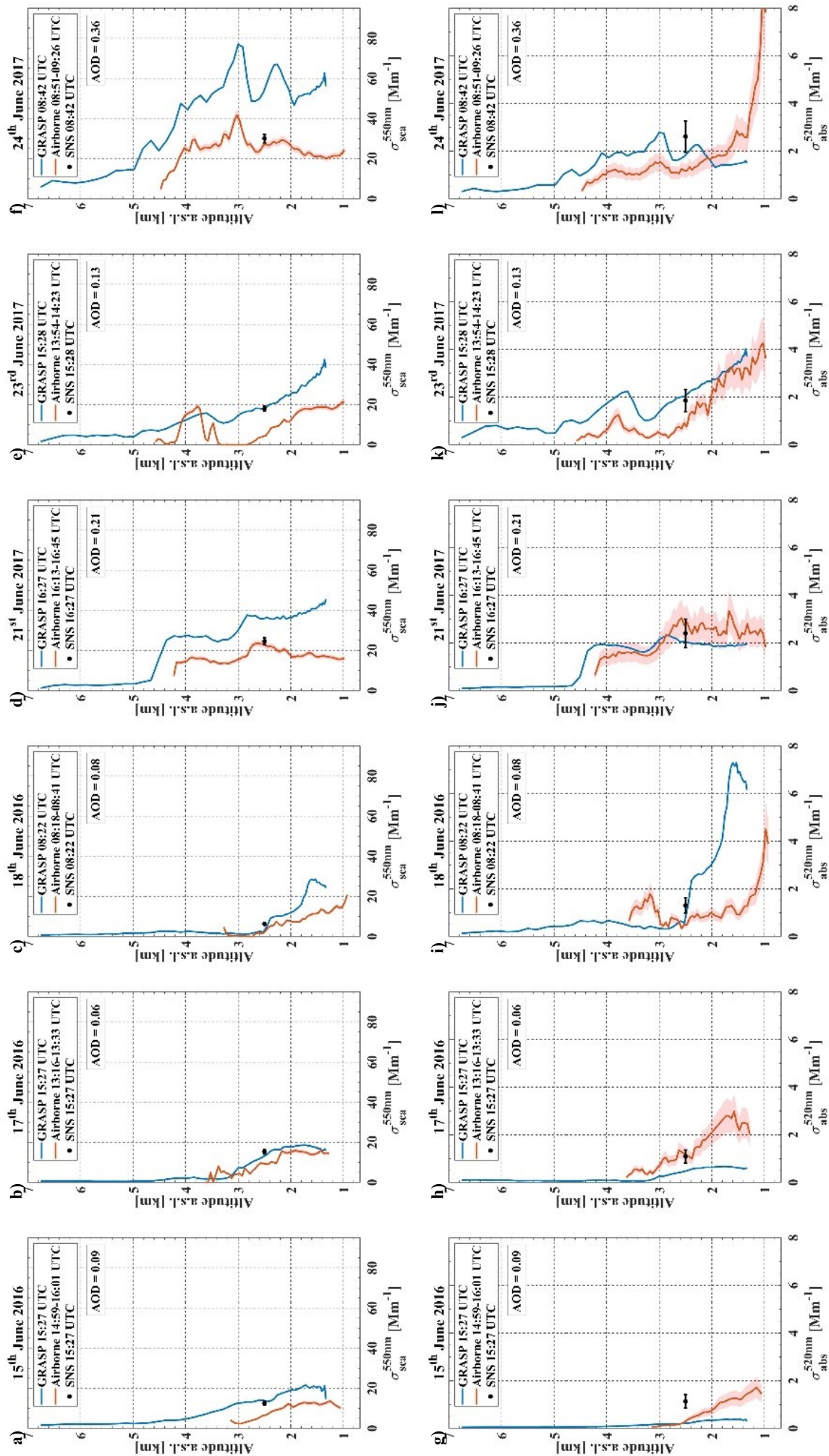
Figure 5. Scattering ($\sigma_{sca}$) and absorption ($\sigma_{abs}$) coefficients at 520 nm retrieved by GRASP (blue), aircraft (red) and SNS (black) in-situ measurements on (**a, g**) 15th, (**b, h**) 17th and (**c, i**) 18th June 2016 and (**d, j**) 21st, (**e, k**) 23rd and (**f, l**) 24th June 2017. The AOD showed is at 440 nm.
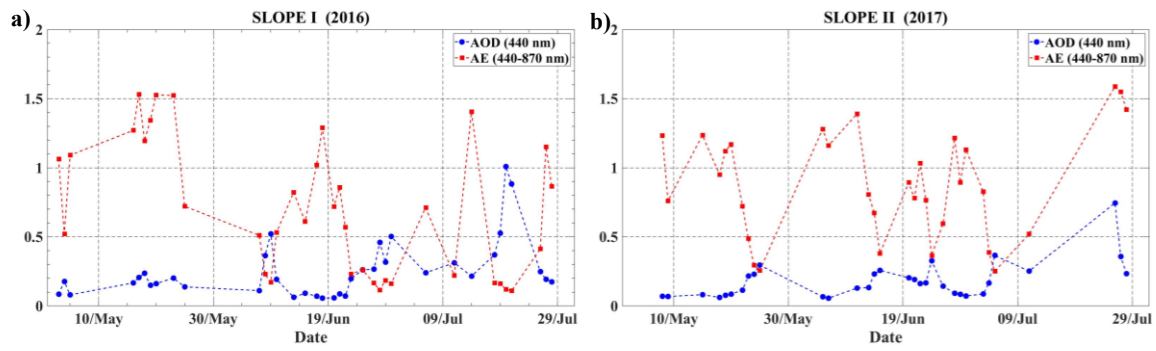
Figure 6. Temporal evolution of aerosol optical depth (AOD) at 440 nm and Ångström exponent (440–870 nm) retrieved by GRASP during (**a**) SLOPE I and (**b**) SLOPE II campaigns.

970
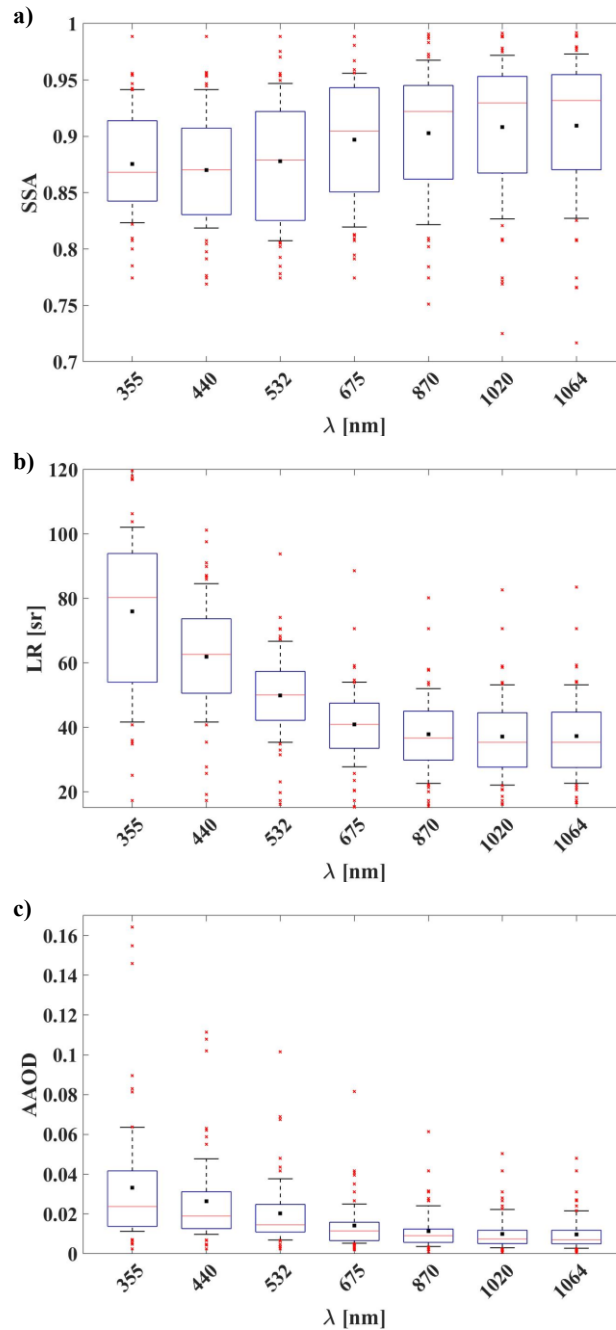
Figure 7. Statistics of (**a**) single-scattering albedo (SSA), (**b**) lidar ratio (LR) and (**c**) absorption aerosol optical depth (AAOD), at 355, 440, 532, 675, 870, 1020 and 1064 nm retrieved by GRASP code during SLOPE I and II campaigns represented as box diagrams. In these box diagrams, the mean is represented by a black dot and the line segment in the box is the median. The bottom and top edges of the box indicate the 25th and 75th percentiles, respectively. In addition, the error bars of the box are the 10th and 90th percentiles, and the crosses represent the outliers values.
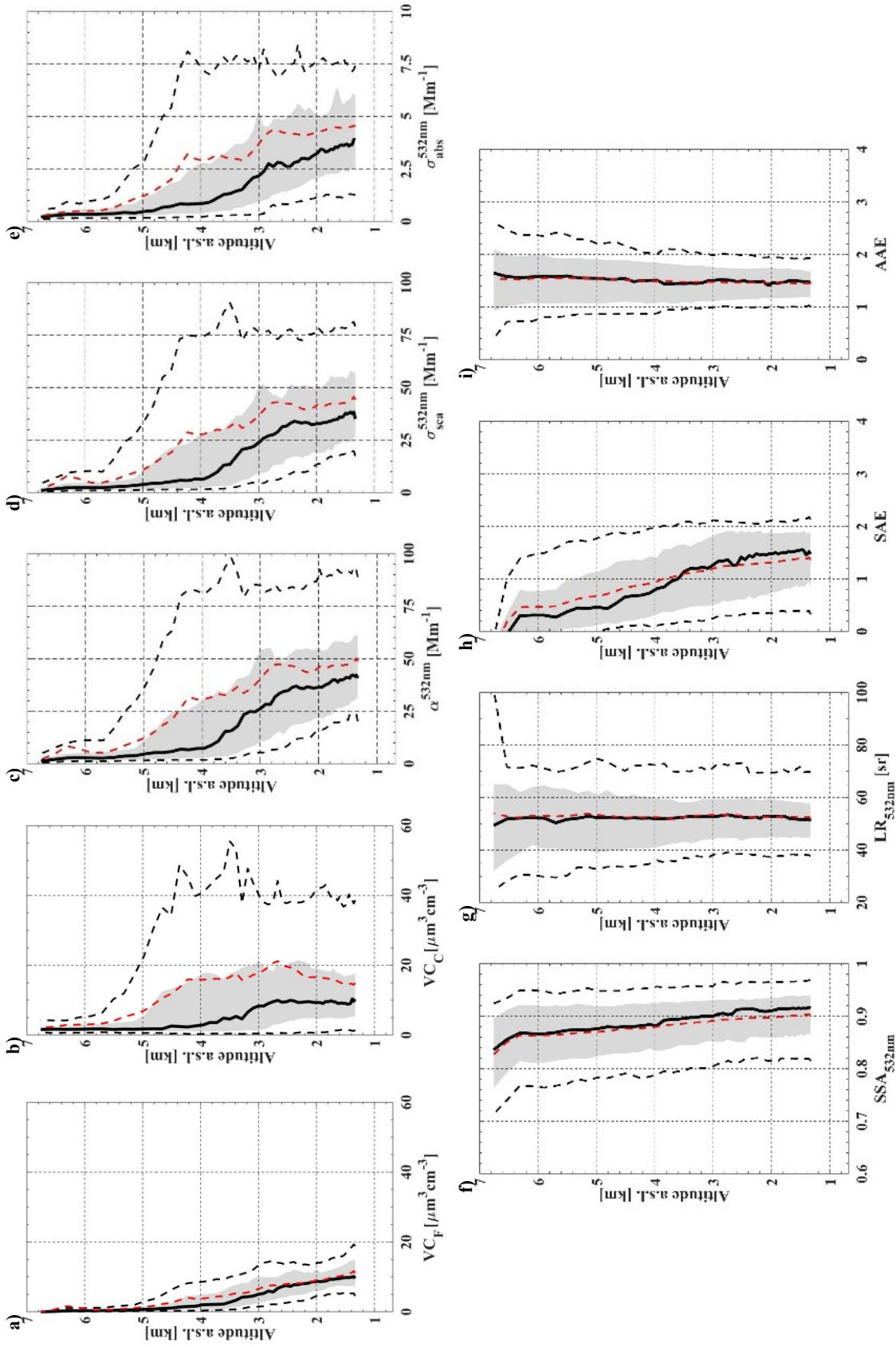
Figure 8. Variability of GRASP vertical profiles: volume concentration for (**a**) fine and (**b**) coarse modes. (**c**) extinction ($\alpha$), (**d**) scattering ($\sigma_{sca}$) and (**e**) absorption ($\sigma_{abs}$) coefficients, (**f**) single-scattering albedo (SSA) and (**g**) lidar ratio (LR) at 532, (**h**) scattering Ångström exponent (SAE) and (**i**) absorption Ångström exponent (AAE) computed between 355 and 1064 nm. The black line represents the median and the red dashed line is the mean. The shadowed area is the interquartile range and the black dashed lines represent the 10th and 90th percentiles. Statistics are based on daily average profiles.
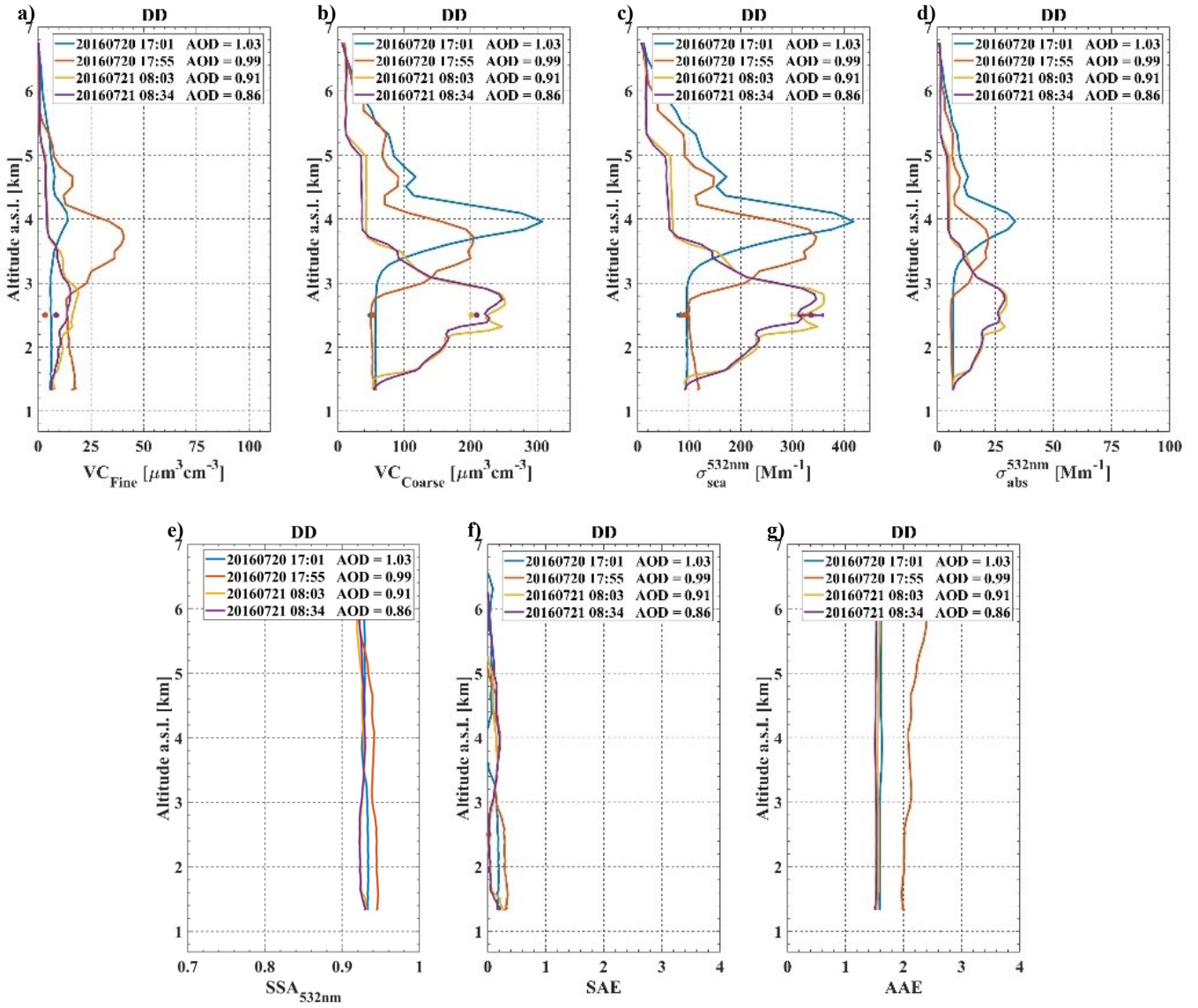
Figure 9. Volume concentration for (**a**) fine and (**b**) coarse modes, (**c**) scattering ($\sigma_{sca}$) and (**d**) absorption ($\sigma_{abs}$) coefficients, (**e**) single scattering albedo (SSA) at 532 nm, (**f**) scattering Ångström exponent (SAE) and (**g**) absorption Ångström exponent (AAE) retrieved by GRASP (line) and SNS measurements (point) during desert dust event on 20th and 21st July 2016. The AOD showed is at 440 nm.

1000
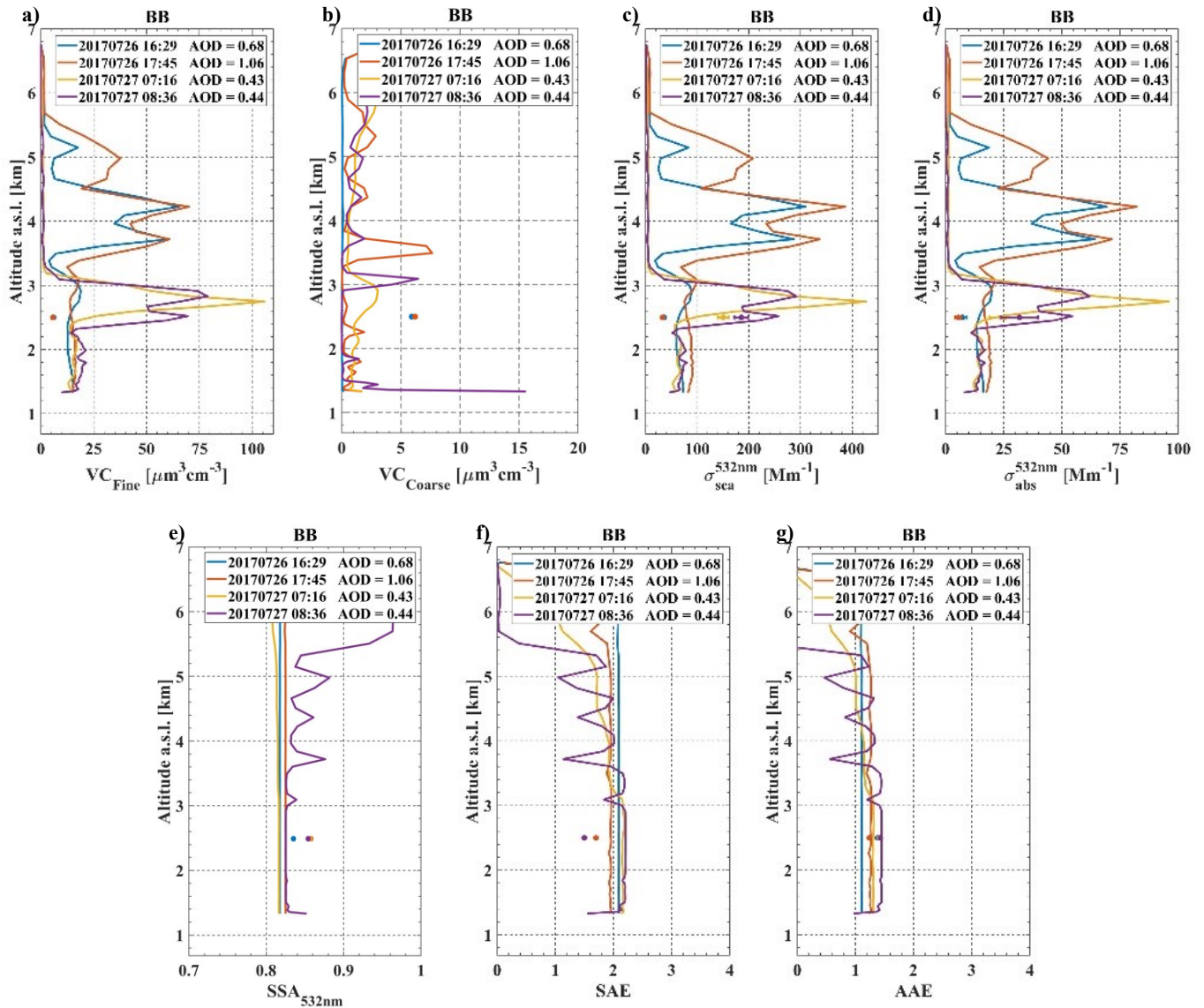
Figure 10. Volume concentration for (**a**) fine and (**b**) coarse modes, (**c**) scattering ($\sigma_{sca}$) and (**d**) absorption ($\sigma_{abs}$) coefficients, (**e**) single scattering albedo (SSA) at 532 nm, (**f**) scattering Ångström exponent (SAE) and (**g**) absorption Ångström exponent (AAE) retrieved by GRASP (line) and SNS measurements (point) during biomass burning event on 26th and 27th July 2017. The AOD showed is at 440 nm.

1005

1010

1015